A boundary element and level set based topology optimisation using sensitivity analysis

B.Ullah*, J.Trevelyan

School of Engineering and Computing Sciences, Durham University,
South Road, Durham DH1 3LE, UK.

Abstract

The structural topology optimisation method presented in this paper is based on the boundary element method, level set method and shape sensitivity analysis for two-dimensional linear elastic problems. The proposed method automatically nucleates holes within the design domain during the optimisation process using a topological derivative based hole insertion criterion. The level set method is used to provide an implicit description of the structural geometry, which is capable of automatically handling topological changes, i.e. holes merging with each other or with the boundary. During the optimisation process non-uniform rational b-splines are fitted through the zero level set contours, which links an implicit geometry representation to its structural model. In addition, this provides an optimal design in standard CAD format, and without intermediate material densities, which can be directly used in other design processes. The proposed optimisation method is tested against different benchmark examples and the optimal geometries generated are in close agreement those available in the literature of topology optimisation.

Keywords: structural optimisation, boundary element method, level set method, NURBS

1. Introduction

The level set method (LSM) is an efficient numerical technique originally developed by Osher and Sethian[1] for the tracking of propagating interfaces

---

*Corresponding author
Email address: baseerullah@gmail.com (B.Ullah)

with topological changes of merging and breaking naturally. There is a wide variety of applications, including structural optimisation, in which LSM has been successfully implemented. Sethian and Wiegmann [2] first presented a level set (LS) based structural optimisation method. In their implementation, shape and topology changes were accomplished through a von Mises stress based criterion. Osher and Santosa [3] proposed a LS based method using shape sensitivity analysis for the optimisation of an inhomogeneous drum for the frequency response. Wang *et al.* [4] also presented a shape sensitivity approach for the solution of minimum compliance problems. Allaire *et al.* [5] independently proposed a LS based optimisation method based on shape sensitivities for the solution of 2D and 3D optimisation problems with both linear and non-linear structural material.

In an LS based optimisation approach, the selection of an effective structural performance measuring tool plays an important role for the solution of optimisation problems. The performance measuring tool predicts the structural response against the applied load and boundary conditions. These responses are then converted into a useful form through shape sensitivity analysis, which informs the evolution of the structural geometry accordingly. The performance of a candidate design can be measured through a geometry mapping technique, which projects the implicitly represented geometry onto the structural model. The most commonly used geometry mapping techniques in the LS based structural optimisation are material distribution (density based), immersed boundary and conforming discretisation [6].

Due to a continuously evolving geometry the standard finite element method (FEM) without re-meshing is not recommended as a structural performance measuring tool in structural optimisation. Therefore, most of the LS based optimisation methods utilise a fixed Eulerian type mesh with an "Ersatz material" approach [5] as an alternative finite element (FE) analysis tool. The structural geometry is represented through a density distribution function, i.e. ($\eta < \rho < 1$) similar to the density based optimisation approach [7]. Solid material is represented by ($\rho = 1$) and holes in the structure are replaced by a specified minimum relative density ($\rho = \eta$). Wang *et al.* [4] and Allaire *et al.* [5] initially implemented the density based approaches in their proposed LS based topology optimisation methods. Although the fixed grid is a simple approach, it is not effective to capture the exact geometry of the boundary [5] and a highly dense grid distribution is always required near the boundary for high accuracy [8]. In addition, the presence of intermediate material densities along the structural boundary can result in non-smooth

2

and indistinct boundary representation [9]. A smoothed Heaviside function approach has been adopted to smooth the discontinuity at the boundary [10, 11]. However, the numerical integration of the stiffness matrix may be less accurate [12].

The second type of geometry mapping is based on the immersed boundary approach, which uses a non-body conforming fixed grid. Therefore, the structural geometry is not aligned with the grid and can intersect some grid cells. This approach allows a clear boundary representation and avoids intermediate density material [6]. Sethian and Wiegmann [2] used the immersed interface method within a finite difference framework for the solution of LS based topology optimisation problems. The extended finite element method (X-FEM) has also been used to evaluate the required properties at the structural boundary through the local enrichment of elements intersected by the zero level set contour [13]. Belytschko *et al.* [14] combined the implicit boundary representation with the X-FEM approach for the solution of topology optimisation problems. The X-FEM has also been used in the LS based optimisation methods presented in [15, 16]. Yamasaki *et al.* [9] developed a two-dimensional topology optimisation method for minimum compliance problems based on the immersed boundary mapping, boundary element and level set methods. The common problem reported in the implementation of immersed boundary methods is the occurrence of small intersection of finite elements [15] or short boundary elements [9] while discretising the structural model. This can profoundly affect the accuracy of structural response. Further, the use of immersed boundary techniques requires sophisticated codes and can make their implementation difficult and time consuming [6].

Some of the LS based optimisation methods use two types of meshes during the numerical implementation, i.e. a fixed Eulerian mesh which maintains the LS function throughout the optimisation process, and a second mesh which exactly fits the design domain. Two different approaches can be used to discretise the design domain, i.e. the domain discretisation (i.e. the FEM) and boundary only discretisation (i.e. the BEM). This third type of mapping provides the most accurate analysis of the structural model and especially along the boundary. The use of BEM with the level set method in two-dimensional structural optimisation was first used by Abe *et al.* [17] for the solution of minimum compliance problems. The proposed approach has also been extended for shape optimisation of sound scattering problems [18]. The use of BEM for acoustic applications has also been thoroughly invitegated in the research work presented in [42, 43, 44]. In those research studies

3

the topological sensitivities are formulated through the BEM framework accelerated with the Fast Multipole method. In the research work of Isakari *et al.* [45] a topology optimisation method was presented through the integration of LSM, Fast Multipole boundary element method and topological sensitivity analysis. The proposed method was applied to three-dimensional wave scattering problems. Ha and Cho [19] utilised an unstructured domain conforming discretisation approach for the optimisation of geometrically non-linear structures within the LS framework. Yamasaki *et al.* [20] presented a boundary tracking approach for the LS based topology optimisation using a conforming discretisation approach and geometry based re-initialisation scheme [21].

In comparison with the immersed boundary mapping, the body conforming approach is attractive due to its simplicity and higher accuracy. However, the domain discretisation based body conforming mapping, i.e. FEM requires special care for a continuously changing structural geometry; that it is difficult to ensure the accuracy of analysis for a continuously changing FE model. However, the boundary based body mapping, i.e. the BEM is attractive because it requires discretisation only at the design boundary (at the zero level set contour). This reduction of problem dimensionality considerably simplifies the re-meshing task (especially in three-dimensions), which can be performed efficiently and robustly. Thus, its rapid and robust re-meshing and accurate boundary solutions make the boundary based body mapping method a natural choice for the solution of LS based shape and topology optimisation problems.

The boundary based body conforming approaches have been progressively improved over the years. However, the research methods presented in the early stages for compliance minimisation, e.g. [9, 17] are based on the initial guessed design with pre-existing holes. Therefore, in the absence of a hole nucleation mechanism, the optimal designs obtained are highly dependent on the initial guessed designs. Ullah *et al.* [22] proposed an evolutionary optimisation approach based on the BEM and LSM with a stress based hole insertion mechanism. The optimal designs generated with their proposed optimisation method do not rely on initial guessed designs with pre-existing holes. The stress based hole insertion criterion is further investigated for a possible correlation with a topological derivative based hole insertion mechanism in [23]. The BEM and LSM based evolutionary optimisation method is further extended for the solution of three-dimensional problems in [24].

The topology optimisation method presented in [22, 23] has been success-

fully implemented with the stress based sensitivities for shape optimisation, and both stress and topological derivative based sensitivities [25, 26] have been used to carry out topological changes. This paper presents a novel methodology where the shape and topological derivatives are used to evaluate the associated sensitivities for compliance minimisation within the BEM and LSM framework. This approach is further equipped with the implementation of a bisectioning algorithm which effectively preserves the volume thereby strictly satisfying the volume constraint. Moreover, the proposed optimisation method does not rely on an initial guessed design with pre-existing holes. Instead the topological derivative based hole insertion criterion [23] used allows automatic hole nucleation and makes this new approach insensitive to the choice of initial guessed design. During the optimisation process NURBS [27] are fitted through the zero level set contours, which links an implicit geometry representation to its structural model. Additionally, this provides an optimal design in a standard CAD format and without intermediate material densities, which can be directly used in other design processes. The proposed method uses the two-dimensional version of the BEM analysis software Concept Analyst (CA) [28]. CA is capable to automatically discretise the NURBS based structural model.

The combination of the BEM (boundary based body mapping) and LSM requires a comprehensive investigation to effectively utilise their attractive properties in the field of structural optimisation. Using this as a milestone, this paper presents a detailed implementation of the use of BEM in a *sensitivity* and LSM based structural topology optimisation. Sections 2 and 3 present overviews of the shape sensitivity analysis and level set based structural optimisation. The BEM is developed in Section 4. We present details of the optimisation algorithm and its implementation in Section 5. The results obtained from the proposed algorithm are presented and discussed in Section 6. The paper closes with some concluding remarks in Section 7.

2. Shape sensitivity analysis

In structural optimisation different objective functions can be used to evaluate the performance of a given structure subject to constraints in the design variables. In this study the design objective function is to find the optimal topology of a structure with minimum compliance subject to a volume constraint. Consider a design domain Ω with a boundary Γ as shown in Figure 1. The boundary Γ is decomposed such that
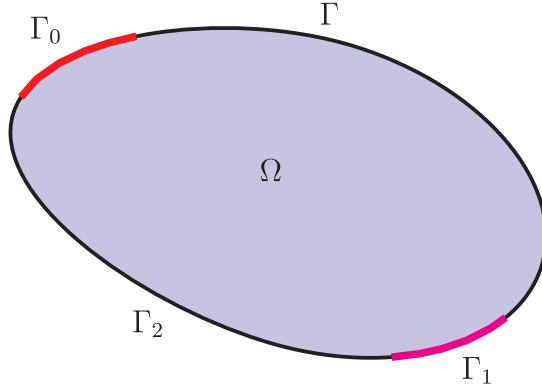
Figure 1: Design domain

$$\Gamma = \Gamma_0 \cup \Gamma_1 \cup \Gamma_2 \tag{1}$$

where Γ_0 corresponds to Dirichlet boundary conditions (where displacements are zeros), Γ_1 corresponds to non-homogeneous Neumann boundary conditions (where tractions are prescribed) and Γ_2 corresponds to homogeneous Neumann boundary conditions (traction free). Γ_0 and Γ_1 are fixed and Γ_2 is allowed to vary during the optimisation process. The objective function is the compliance (i.e. a measure of the strain energy) given in [29] as

$$J(u) = \int_\Gamma \frac{1}{2} t_i u_i d\Gamma \tag{2}$$

where t_i and u_i are the traction and displacement components in the direction i. The optimisation problem can be expressed as finding Γ_2 to minimise $J(u)$, subject to the volume constraint

$$G = \int_\Omega d\Omega - V = 0 \tag{3}$$

where V is the target volume.

According to Soares and Choi [29], for a linear material the first variation of the objective function, (i.e. Equation (2)) becomes

$$J'(u) = -\int_{\Gamma_2} W v_n d\Gamma \tag{4}$$

where W is the strain energy density and v_n is the normal velocity of the boundary, here W is

$$W = \frac{1}{2}\, \sigma_{ij}\, \epsilon_{ij} \tag{5}$$

6

where σ_{ij} and ϵ_{ij} are the stress and strain components, respectively. Similarly, the variation of the constraint functional (i.e. Equation (3)) given in [29] is

$$G' = \int_{\Gamma_2} v_n d\Gamma \tag{6}$$

Soares and Choi [29] used the Pshenichny linearisation method [30] of linear programming in combination with the boundary element method to solve the optimisation problem. However, the optimisation problem can also be solved with the Lagrange multiplier method as:

$$\bar{J}(u) = J(u) + \ell G \tag{7}$$

where ℓ is a positive Lagrange multiplier and $\bar{J}(u)$ is the modified objective function. The Karush-Kuhn-Tucker (KKT) optimality conditions require that for an optimal solution (or for a minimiser), the following conditions must be satisfied.

$$\bar{J}'(u) = 0 \tag{8}$$

Finally, the variation of the Lagrangian can be written as

$$\bar{J}'(u) = \int_{\Gamma_2} (\ell - W) v_n d\Gamma \tag{9}$$

3. Level set based structural optimisation

The LSM uses the Eulerian approach to represent an evolving geometry implicitly. In a level set (LS) based structural optimisation, the structural geometry is first embedded as the zero level set of a higher dimensional function ϕ. This method works on an underlying fixed Cartesian grid. In most cases, the initial function ϕ is defined as the distance of a particular grid point from the boundary with a sign to indicate points either inside or outside of the boundary. These definitions are expressed as follows and shown in Figure 2.

$$\phi(\vec{x}) \begin{cases} < 0 & \vec{x} \in \Omega \\ = 0 & \vec{x} \in \partial\Omega \text{ or } \Gamma \\ > 0 & \vec{x} \in \Omega_H \end{cases} \tag{10}$$

where $\vec{x}$ is a point within the level set domain; Ω represents the region contained within the boundary, Ω_H as the union of the regions inside holes
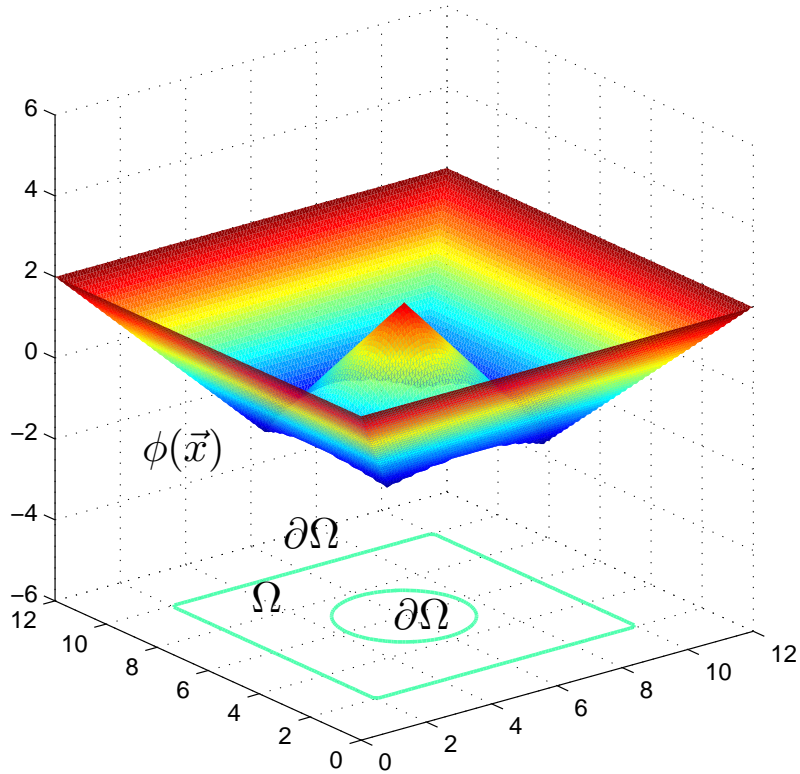
7

Figure 2: Geometry implicit representation

and the region of the design domain outside the boundary, and the contour $\partial\Omega$ as the interface between the non-overlapping regions Ω and Ω_H.

The propagation of the structural boundary during the optimisation iterations can be linked with the evolution of ϕ as an initial value problem. This means that the position of the structural boundary at any time t is given by the zero level set of the function ϕ. A change in ϕ will modify the structural geometry accordingly. The level set function ϕ can be evolved through the solution of a Hamilton-Jacobi (HJ) equation [1]

$$\frac{\partial\phi}{\partial t} + v_n|\nabla\phi| = 0 \qquad (11)$$

where v_n is the velocity in the normal direction and t is the virtual time. The

normal velocity along the boundary can be computed from the structural response, e.g shape sensitivity analysis ([4, 5]).

Equation (9) indicates that the shape derivatives can be easily obtained with surface integration. However, the LSM depends only on the normal velocity v_n and the calculation of surface integration is unnecessary [10]. A descent direction for the Lagrangian can be obtained by simply identifying the normal velocity v_n as [5, 10, 31]

$$v_n = W - \ell \tag{12}$$

where v_n at the moving free boundary Γ_2 can be computed from the strain energy density and Lagrange multiplier. In the present study the strain energy density can be accurately and efficiently calculated using the BEM, which requires boundary elements on the zero level set contours and avoids geometric approximation at the boundary as adopted for the fixed grid type approaches usually employed [5, 10, 31]. The calculation of Lagrange multiplier ℓ used for the computation of v_n is discussed in Section 5.3.

4. Boundary element method

The Boundary Element Method (BEM) is a standard technique for computational solution of partial differential equations. There are numerous textbooks describing the method (e.g. Becker [32]), but for completeness a brief description is included in this section.

We consider linear elasticity in the domain $\Omega \subset \mathbb{R}^2$, having boundary $\partial\Omega = \Gamma$. The boundary includes an exterior boundary and may contain interior boundaries to model holes in the structure. These will be important as design topologies develop. We solve the equilibrium equations

$$\sigma_{ij,j}(\vec{x}) + b_i(\vec{x}) = 0, \qquad \vec{x} \in \Omega \tag{13}$$

where $i, j = x, y$, the problem being subject to boundary conditions

$$u_i(\vec{x}) = \bar{u}, \qquad \vec{x} \in \Gamma_0 \tag{14}$$

$$t_i(\vec{x}) = \bar{t}, \qquad \vec{x} \in \Gamma_1 \tag{15}$$

In the above, u_i represents a displacement component, σ the Cauchy stress tensor and b the body force vector. The boundary $\Gamma = \Gamma_0 \cup \Gamma_1 \cup \Gamma_2$, but since it is commonplace in practice to prescribe different boundary condition

9

types in different coordinate directions at the same point, this definition is purely symbolic. The traction component, t_i, is given by

$$t_i(\vec{x}) = \sigma_{ij}(\vec{x})n_j(\vec{x}), \qquad \vec{x} \in \Gamma \qquad (16)$$

where n is the unit outward pointing normal vector at $\vec{x}$. The terms $\bar{u}, \bar{t}$ are prescribed known displacements and tractions respectively. The Einstein summation convention is assumed throughout. Taking for simplicity here the case $b = 0$, the differential equations (13) can be transformed into an equivalent integral equation form known as the Somigliana identity. We may write

$$c_{ij}(\vec{x})u_j(\vec{x}) + \fint_{\Gamma} T_{ij}(\vec{x}, \vec{y})u_j(\vec{y})d\Gamma(\vec{y}) = \int_{\Gamma} U_{ij}(\vec{x}, \vec{y})t_j(\vec{y})d\Gamma(\vec{y}) \qquad (17)$$

where T_{ij}, U_{ij} are respectively the traction and displacement kernels, or fundamental solutions. The free coefficients, c_{ij}, arise from the strong singularity in the integral containing the traction kernel; this integral is denoted $\fint$ to indicate its evaluation in the Cauchy Principal Value sense. The boundary may be discretised using elements, i.e.

$$\Gamma = \bigcup_{e=1}^{N_e} \Gamma_e, \quad \Gamma_i \cap \Gamma_j = \emptyset, i \neq j \qquad (18)$$

and the geometry of each element parameterised in terms of a local intrinsic coordinate $\xi^e \in [-1, 1], e = 1, ..., N_e$, allowing (17) to be rewritten

$$c_{ij}(\vec{x})u_j(\vec{x}) + \sum_{e=1}^{N_e} \sum_{l=1}^{m} \left[\int_{-1}^{+1} T_{ij}(\vec{x}, \vec{y}(\xi^e))N_l(\xi^e)J^e(\xi^e)\,d\xi^e \right] u_j^{el}$$

$$= \sum_{e=1}^{N_e} \sum_{l=1}^{m} \left[\int_{-1}^{+1} U_{ij}(\vec{x}, \vec{y}(\xi^e))N_l(\xi^e)J^e(\xi^e)\,d\xi^e \right] t_j^{el} \qquad (19)$$

where l is a local node number, on element e, that varies from 1 to $m = 2, 3, ...$ for linear, quadratic elements etc., $\vec{y}$ is the location on the element corresponding to the variable of integration ξ^e, N_l is the Lagrangian shape function for node l, $J^e = d\Gamma_e/d\xi^e$ is the Jacobian of transformation and u_j^{el} and t_j^{el} are displacements and tractions, respectively, at local node l on element e. Taking point $\vec{x}$ to be a node point, and evaluating the boundary

integrals in (19) using a suitable scheme that copes with the singularities in the fundamental solutions, we arrive at

$$c_{ij}(\vec{x})u_j(\vec{x}) + \sum_{e=1}^{N_e}\sum_{l=1}^{m} h^{el} u_j^{el} = \sum_{e=1}^{N_e}\sum_{l=1}^{m} g^{el} t_j^{el} \tag{20}$$

where h^{el}, g^{el} are the evaluated integrals. Finally, placing point $\vec{x}$ at each node in turn, equations of this form may be developed at each, and these may be assembled to form a linear system

$$[\mathbf{H}]\{\mathbf{u}\} = [\mathbf{G}]\{\mathbf{t}\} \tag{21}$$

where the matrices $\mathbf{H}$ and $\mathbf{G}$ contain the coefficients h^{el} and g^{el} respectively, and multiply vectors of nodal displacements and tractions. Application of the boundary conditions (14) and (15) reduces the problem to a square system that can be solved for unknown boundary displacements and tractions.

It is important in topology optimisation to determine accurate solutions at *internal points*, i.e. points $\vec{x} \in \Omega\backslash\Gamma$. Once equation (21) has been solved, internal point displacements can be found using (19) by taking $\vec{x}$ as the point in question and letting $c_{ij} = \delta_{ij}$, where δ_{ij} is the Kronecker delta, and likewise stress components may be determined from a differentiated form of the same expression.

5. Optimisation algorithm

In the previous BEM and LSM based optimisation approaches presented in [9, 17], initial guessed designs with pre-existing holes have been considered for the solution of minimum compliance problems. However, due to the absence of a hole nucleation mechanism, optimal designs obtained with those methods are highly dependent on the initial guessed designs. In this new implementation, a topological derivative based hole insertion criterion has been proposed, which automatically inserts holes during the optimisation process. The proposed algorithm is depicted in Figure 3. It can be seen that in this new algorithm the user is allowed to switch ON/OFF the hole insertion option during the optimisation process. Hence, the addition of the hole insertion option allows the freedom to use initial guessed designs with or without pre-existing holes for the solution of the minimum compliance problem.
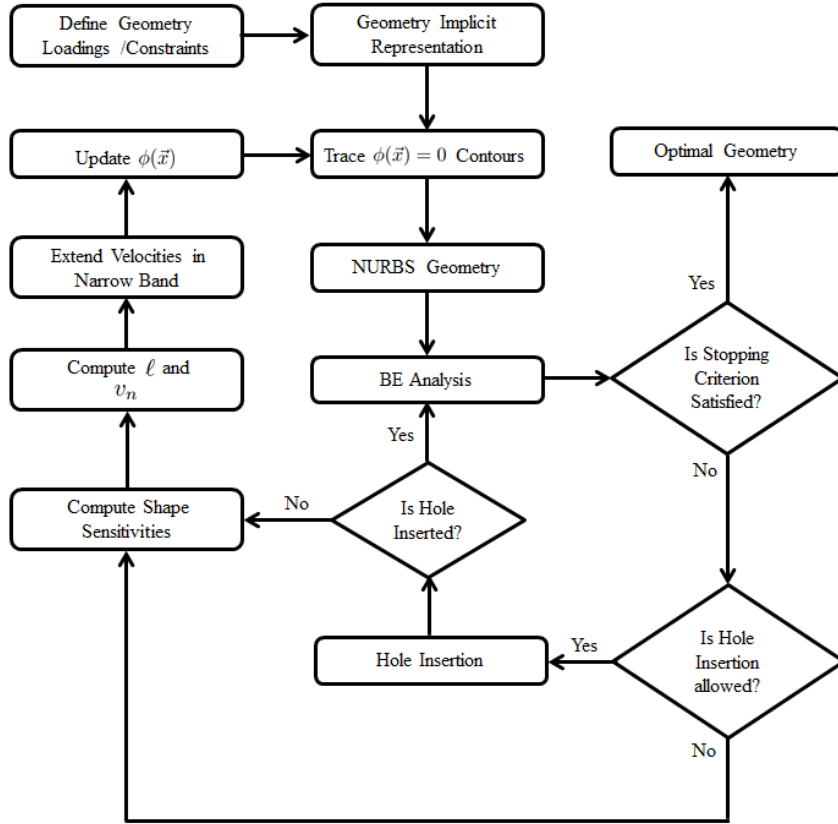
Figure 3: Optimisation flow chart

5.1. Structural geometry representation: from implicit to NURBS

The proposed optimisation method is based on two different types of discretisation. The first type uses a fixed Eulerian discretisation, which maintains the level set function throughout the optimisation process, whereas, the second type of discretisation fits exactly the structural geometry. During the optimisation process shape changes are governed by the evolution of the LS function, which is based on the implicit boundary representation. At each optimisation iteration the modified geometry needs to be analysed for its structural response. Therefore, a structural model is always required at each optimisation iteration. This section discusses the mechanism which links an implicit geometry representation to its structural model.

In the first step a rectangular level set domain Ω_L is defined to capture

all the possible geometry changes during the optimisation process. The dimensions of Ω_L used in the current implementation are slightly bigger than the structural geometry Ω. Design domain Ω_L is discretised with a suitable level set grid size, d. Once the initial geometry is defined the level set grid is initialised with a signed distance function in accordance with Equation (10).

During the optimisation process, at each iteration, the solution of Equation (11) updates $\phi(\vec{x})$, which allows us to modify the structural geometry. The $\phi(\vec{x}) = 0$ contours (which represent the boundary of the modified geometry) need to be reconstructed from the level set grid. Therefore, in the next step the positions of the zero level set intersection points are calculated with a linear interpolation scheme. Figure 4(a) and (b) display the zero level set intersection points calculated for an initial and intermediate geometry of a squared shape short cantilever beam. It can be seen that the adjacent intersection points are equidistant in the case of an initial geometry, whereas, the distance varies between the adjacent points for the intermediate geometry.

(a) Initial geometry   (b) Intermediate geometry
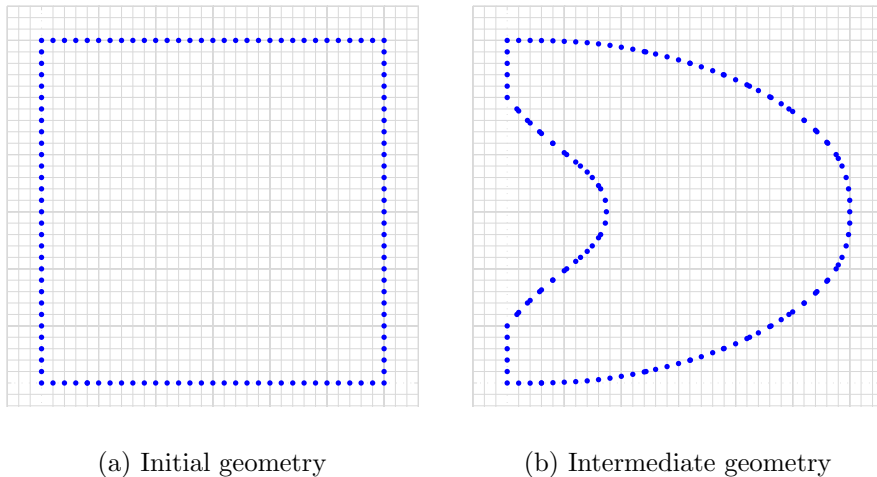
Figure 4: Zero level set intersection points for a squared shape short cantilever beam

In order to reconstruct the geometry, straight line segments are used to connect the zero level set intersection points as shown in Figure 5(a). This yields a non-smooth polygonal structural geometry with line segments of non-uniform length. In the BE analysis if the zero level set intersection points are directly used as element nodal points (as in [9]), two intersection points can lie very close to each other (for example see Figure 5(a)), which can cause

difficulties and instabilities during the BE analysis. A better solution proposed in [22] is to fit a NURBS curve through those zero level set intersection points which belong to Γ_2. Figure 5(b) and (c) shows the resulting NURBS curves fitted through the zero level set intersection points, where each curve exactly passes through maximum number of intersection points.

The automatic meshing facility within the CA software is used to define elements on each spline, using a setting which is designed to produce peak stresses to approximately 1% accuracy, either with uniformly distributed boundary elements with mid side nodes as shown in Figure 5(d) or with grading as required for good BEM meshing practice. It can be seen that with a NURBS based geometry representation, BE meshing can be carried out independently of the level set grid size. This provides the freedom to use a suitable grid size based on the required accuracy and computational efficiency during the numerical implementation of the proposed method.

At each optimisation iteration a BE analysis is carried out for the modified structural geometry, which is then followed by sensitivity calculations and hole insertion check.

5.2. Hole insertion and sensitivity calculations

In a BE analysis stresses/strains within the structure are calculated at internal points. In the numerical implementation, level set grid points with $\phi(\vec{x}) < 0$ are used as internal points and hence this provides a regular grid of these points.

In the proposed optimisation method the hole insertion criterion is based on the topological derivative approach. The original concept of topological derivative is related to the sensitivity of a cost function when material is removed from the design domain through a small hole insertion. However, the difficulty of establishing a direct mapping between the two different domains (i.e. the domain with and without a hole) restricts its implementation in an optimisation problem. Novotny *et al.* [33] presented an alternative approach to overcome the difficulty associated with the original definition. Based on this new approach, a hole creation is equivalent to the idea of perturbing a pre-existing hole, whose radius tends to zero, thereby providing the possibility to establish a direct mapping between the initial and modified domains. This idea has been used for the derivation of the most useful and easy to implement formulation of the topological derivative (see for details [33, 46]). In a BEM framework this concept has been used by Carretero and Cisilino [26], and Marczak [34], for the optimisation of 2D elasticity problems with the total

14

(a) Reconstructed geometry

(b) NURBS through intersection points

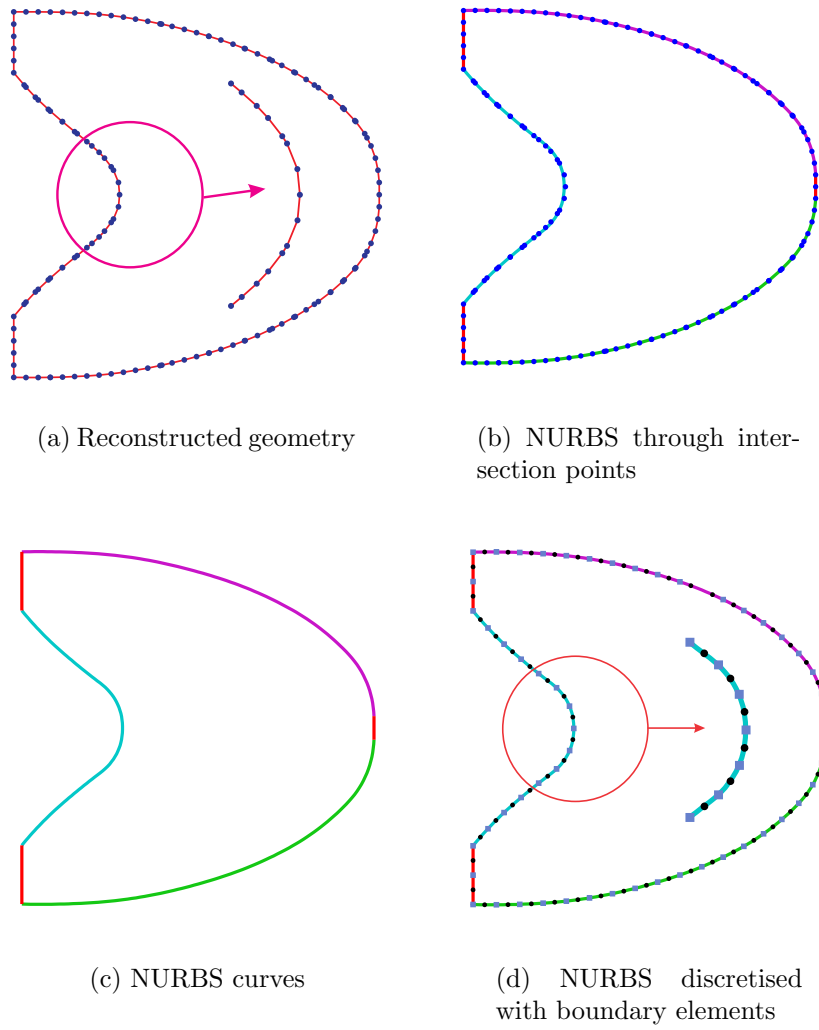(c) NURBS curves

(d) NURBS discretised with boundary elements

Figure 5: Re-constructed geometry

strain energy as the cost function. According to [33, 46], the topological derivative $D_T(\vec{x})$ can be written as a function of stress invariants, i.e.,

$$D_T(\vec{x}) = \frac{4}{1+\nu} \, \sigma \cdot \epsilon + \frac{3\nu - 1}{(1-\nu^2)} \, \mathrm{tr}\sigma \mathrm{tr}\epsilon \tag{22}$$

where ν is the Poisson's ratio, $\mathrm{tr}\sigma$ and $\mathrm{tr}\varepsilon$ represent the trace of stress and strain tensors, respectively. The removal of material within the design domain is based on the topological derivative based hole insertion criterion proposed in [23], according to which holes are inserted in the design domain around the internal points satisfying the following condition:

$$D_T(i) \leq \, f_T \, D_{Tmin} \tag{23}$$

where $D_T(i)$ is the topological derivative at a given internal point i, D_{Tmin} is the minimum value of topological derivative over all internal points in the current iteration and f_T is the topological derivative threshold factor. The selection of f_T and other relevant parameters adopted in this study, for hole insertion, are based on the comprehensive investigation carried out by the authors in their earlier research work presented in [22, 23].

At each optimisation step a hole insertion check is carried out after the BE analysis; holes are automatically inserted once the hole insertion criterion is fulfilled. A BE analysis is carried out after each hole insertion followed by a hole insertion check. In case there is no more hole insertion the shape sensitivities are calculated at the structural boundary as a post processing step.

In order to evolve the structural geometry, normal velocities at the boundary need to be calculated using Equation (12). However, a necessary condition for the solution of (12) requires the Lagrange multiplier ℓ to be known in advance. In the present implementation, the bisectioning algorithm is used for the calculation of ℓ. The following section is devoted to the implementation details of the bisectioning algorithm.

5.3. Bisectioning algorithm and computation of v_n

Allaire *et al.* [5] and Wang and Wang [35] used a fixed value of ℓ for the solution of Equation (12). However, the selection of a fixed ℓ during the optimisation process cannot guarantee exact satisfaction of the volume constraint and only unconstrained optimisation can be performed [10]. In the literature different methods have been proposed for the calculation of

16

ℓ to exactly satisfy the volume constraint during the optimisation process, e.g. Newton's method [3, 4, 31]. Similar to the SIMP method [36], Wang *et al.* [10] implemented a bisectioning algorithm for the calculation of ℓ which exactly satisfies the volume constraint during an LSM based optimisation process. An approach similar to the one proposed by Wang *et al.* [10] has been used in this study to calculate ℓ for the solution of Equation (12) at each optimisation iteration.

During the optimisation process, the material volume is a monotonically decreasing function of ℓ. Using Equation (12), the shape derivative for the volume constraint, i.e. (6) can be re-written as [10]

$$\acute{G} = \int_{\Gamma_2} (W - \ell)d\Gamma \tag{24}$$

It is evident from (24) that the value of $\acute{G}$ increases with a low value of ℓ and decreases with a higher one. In other words, two different values, i.e. ℓ_1 and ℓ_2 can be used to set a lower and an upper bound for ℓ, i.e. $\ell_1 \leq \ell \leq \ell_2$. This suggests that when $\ell = \ell_1$, v_n will be positive, and the structural boundary will move in the outward direction, and this will increase the volume. Similarly, with $\ell = \ell_2$, v_n will become negative and the structural boundary will move inward, and the volume will be decreased. According to [36], the interval between ℓ_1 and ℓ_2 is repeatedly halved at a given iteration until it satisfies the convergence criterion for the volume constraint. In the proposed method the bisectioning algorithm is initialised with suitable values of ℓ_1, and ℓ_2. The implementation details of the bisectioning algorithm are given below.

1. Initialise ℓ_1 and ℓ_2
2. Set $\bar{\phi} = \phi$
3. Halve the interval, i.e.

$$\ell = (\ell_1 + \ell_2)/2 \tag{25}$$

4. Calculate v_n for all boundary points using Equation (12)
5. Extend velocities to the grid points around the narrow band (See Section 5.4)
6. Update the level set function (See Section 5.4), i.e, solve

$$\frac{\partial \bar{\phi}}{\partial t} + v_n|\nabla \bar{\phi}| = 0 \tag{26}$$

to give updated values of $\bar{\phi}$ at the LS grid points.

17

7. Trace the zero level set contours
8. Calculate the new volume
9. if $G > 0$ $\ell_1 = \ell$, otherwise $\ell_2 = \ell$
10. Terminate if $|\ell_2 - \ell_1| \leq 10^{-2}$, otherwise go to step 2.
11. Set $\phi = \bar{\phi}$

During the optimisation iterations, the above algorithm is used for the calculation of the value of ℓ which exactly satisfies the volume constraint. Wang *et al.* [10] proposed that the normal velocities calculated at a constant volume act as mass conservative velocities and hence, this level set method can be generally considered as mass conservative.

In the numerical implementation, it has been observed and as reported in [10], that in the early iterations, when the domain volume still greatly exceeds the target volume, it is possible to remove larger amounts of material in a single step than in later iterations. However, this may cause significant topological changes with some undesirable results. Therefore, in those situations, a fixed value of ℓ can be selected, so that the optimisation can progress more efficiently in the early stages, and the bisectioning algorithm can be used afterwards, which calculates the correct ℓ to exactly satisfy the volume constraint.

5.4. Velocity extension and update of the level set function

Once the velocities are calculated at each node point along the boundary, in the next step these velocities are extended to the level set grid using the method developed by Adalsteinsson and Sethian [37]. This method works on the simultaneous construction of the temporary signed distance function ϕ_t and extension velocity v_{ext} as follows,

$$\nabla \phi_t \, . \, \nabla v_{ext} \, = \, 0 \qquad (27)$$

The Fast Marching Method [38] is used for the construction of ϕ_t, which is based on the solution of the following Eikonal equation,

$$|\nabla \phi_t| \, = \, 1 \qquad (28)$$

In the current BEM based implementation, the normal velocity is directly available at the structural boundary and can be easily extended to the whole design domain as in the case of [5]. However, a narrow band approach [39] adopted in this study allows extension of the normal velocity to few grid

points around the boundary, which is computationally more efficient than that used in [5]. After the velocity extension, the level set function is updated through the solution of Equation (11) with an upwind finite difference approximation [38]. The value of time step size used in Equation (11) is based on the Courant-Friedrichs-Lewy (CFL) condition.

6. Examples

The validity and efficiency of the sensitivity based optimisation method are tested against some benchmarking problems in the field of structural optimisation. The material properties used in these examples are: Poisson's ratio = 0.3, Young's modulus = 210 GPa, Yield stress = 280 MPa. Plane stress conditions are assumed with arbitrary thickness of 1 mm. All examples are solved with a load $P = 100$ N. A time step size $dt = 0.0001$ is used throughout the numerical implementation. In order to capture all possible boundary movements a fixed level set domain is used during the numerical implementation with size slightly larger than the initial design domain. The optimisation process terminates when the relative difference between the compliances of the five successive iterations are less than 10^{-2} or when the given maximum number of iterations has been reached.

6.1. Example-1

The first example considered in this study is a cantilever beam with an aspect ratio of 2:1. As discussed in Section 3, the proposed approach is capable of inserting holes during the optimisation process and also allows the freedom to switch ON/OFF the hole insertion during the optimisation process. Therefore, in this example three different options are considered for the solution of the minimum compliance problem as follows:

1. Initial design with pre-existing holes and without hole insertion
2. Initial design with pre-existing holes and with hole insertion
3. Initial design without pre-existing holes and with hole insertion

In the first case the initial design with applied load and boundary conditions is shown in Figure 6(a). The structure is constrained at the top and bottom of the left hand edge with zero displacement boundary conditions and load P is applied at the middle of right hand edge. The traction free boundary, i.e Γ_2 is allowed to vary during the optimisation process. The minimum compliance problem is solved for a target volume $V = 0.5V_0$ (where

19

V_0 is the volume of initial design domain) and the hole insertion option is switched OFF.

(a) Initial Design

(b) Iteration 20

(c) Iteration 30

(d) Iteration 40

(e) Iteration 60

(f) Iteration 220
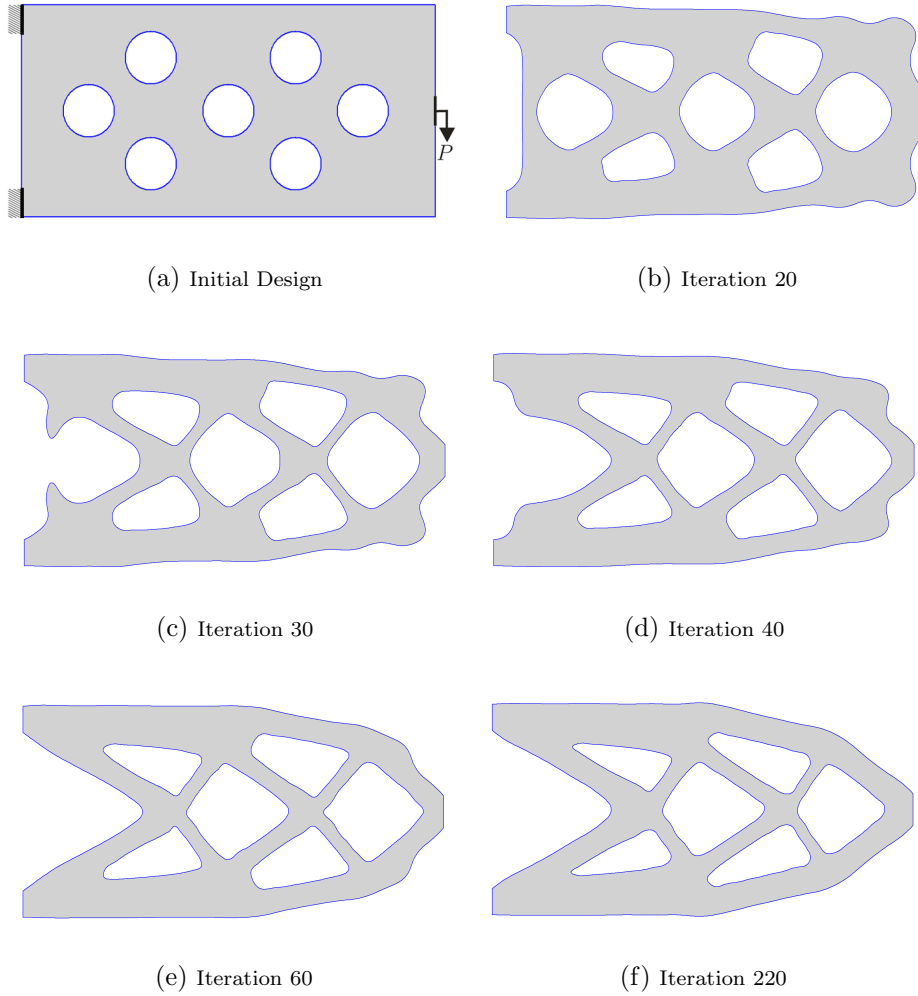
Figure 6: Evolution of structural geometry for Example-1, initial design with pre-existing holes and without hole insertion

The level set domain is discretised with 80×40 square cells. The volume of the initial design domain is $0.87V_0$, which is far away from the target volume, so that (as discussed in Section 5.3), a fixed value of ℓ is used initially to provide a smooth progression towards the target volume. Afterwards, at each optimisation step an appropriate value of ℓ is determined through the use of

20

the bisectioning algorithm which exactly satisfies the volume constraint.

Results obtained at different stages of the optimisation process are depicted in Figure 6. It can be seen that during the optimisation process, the structural geometry evolves into an optimal design through boundary movements and merging of one of the holes with the outer boundary. Moreover, design topologies at iteration 40 and 200 suggest that once the volume constraint is satisfied the proposed optimisation method efficiently redistributes material within the design domain mainly through shape optimisation. The optimal geometry depicted in Figure 6(f) is very similar to those available in the literature, e.g. [5, 10, 35]. Throughout the optimisation process the traction free boundary of the design domain is represented with NURBS (i.e. in a standard CAD format) and hence this allows that the optimal geometry can be directly used in other design processes.

Figure 7 shows the convergence histories of the objective function and volume of the structure during the optimisation process. In the initial 22 iterations, the use of a fixed ℓ provides a smooth progression of the structural geometry. In the subsequent iterations, once the structural volume reaches near the target volume, the bisectioning algorithm is used to calculate ℓ. This results in a rapid decrease in the volume and a corresponding increase in the compliance of the structure. The compliance of the initial design is 1.23 and the material removal increases this value to 1.75. Once the volume constraint is exactly satisfied, the topological changes take place at constant volume, the compliance decreases in a stable manner to 1.42, and remains stable in the following iterations. The optimisation process terminates at iteration 220 where the stopping criterion is satisfied.

In order to evaluate the hole insertion capabilities of the proposed method with an initial guessed design with pre-existing holes the same initial design as considered earlier in this example (i.e. Figure 6(a)), is used and hole insertion option is switched ON. The proposed method allows nucleation of holes using the topological derivative approach (see for detail [23]). A typical value of $f_T = 1.5$ is used in this example. The evolution of the structural model at different stages of the optimisation process is depicted in Figure 8. Nucleations of some new holes can be observed in Figures 6(b), (c), (e) and (f). For comparison purpose the same number of iterations are used as in the first case of this example, and a very similar optimal design has been achieved as shown in Figure 8(h).

The evolution of the objective function and volume of the structure with the hole insertion option switched ON, is depicted in Figure 9. It can be
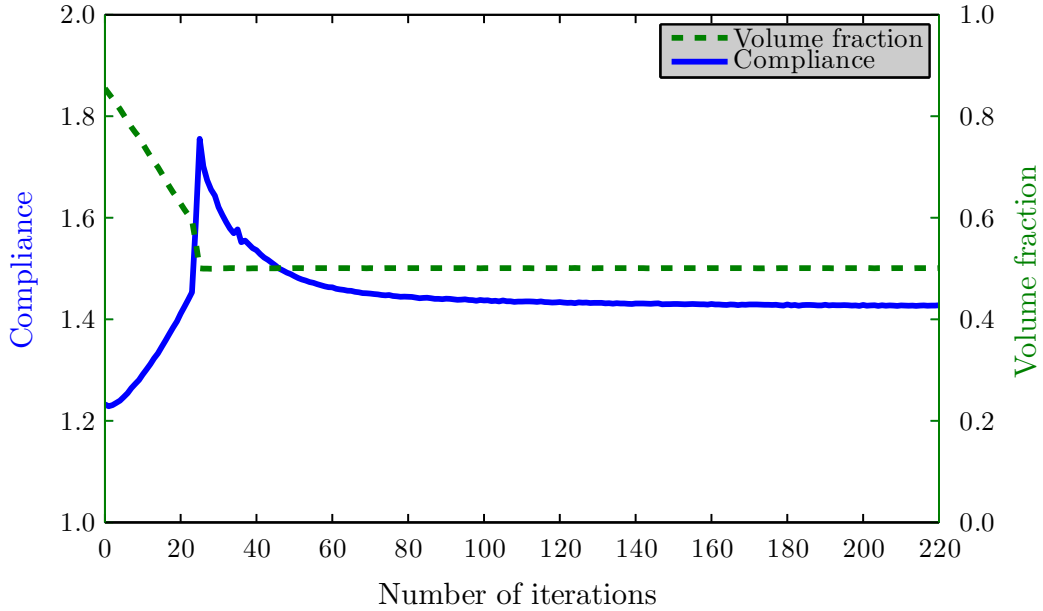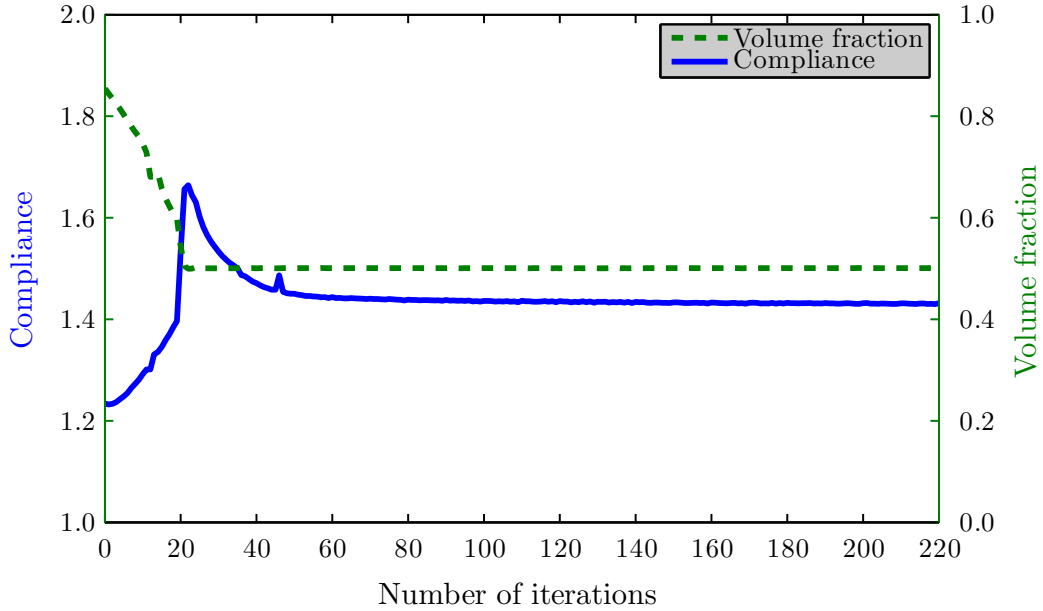
Figure 7: Convergence of objective function and volume for Example-1, initial design with pre-existing holes and without hole insertion

seen that hole insertion slightly accelerates the volume convergence, i.e. 25 iterations were used in the first case, whereas 20 iterations have been utilised in the present case. The optimisation process terminates with a final value of 1.43 which is very close to the first case, i.e 1.42.

In order to further evaluate the hole insertion capability of the proposed method and insensitivity to initial guessed designs, the minimum compliance problem is further solved with an initial design without pre-existing holes as shown in Figure 10(a). Hole insertion is allowed during the optimisation process with $f_T = 1.35$. It should be noted that a larger value of f_T used in the previous case of this example is due to the pre-existing holes in the initial design, which required slightly larger value to insert more holes during the optimisation process. It is evident from the optimisation history depicted in Figure 10, that the current optimisation method nucleates holes at appropriate locations with size varying according to the topological sensitivities. The use of the LSM efficiently handles topological changes, i.e. hole merging with each other and with the outer boundary throughout the optimisation process. The final solution is very similar to the optima of the initial two

22

(a) Initial Design

(b) Iteration 11

(c) Iteration 12

(d) Iteration 14

(e) Iteration 16

(f) Iteration 37

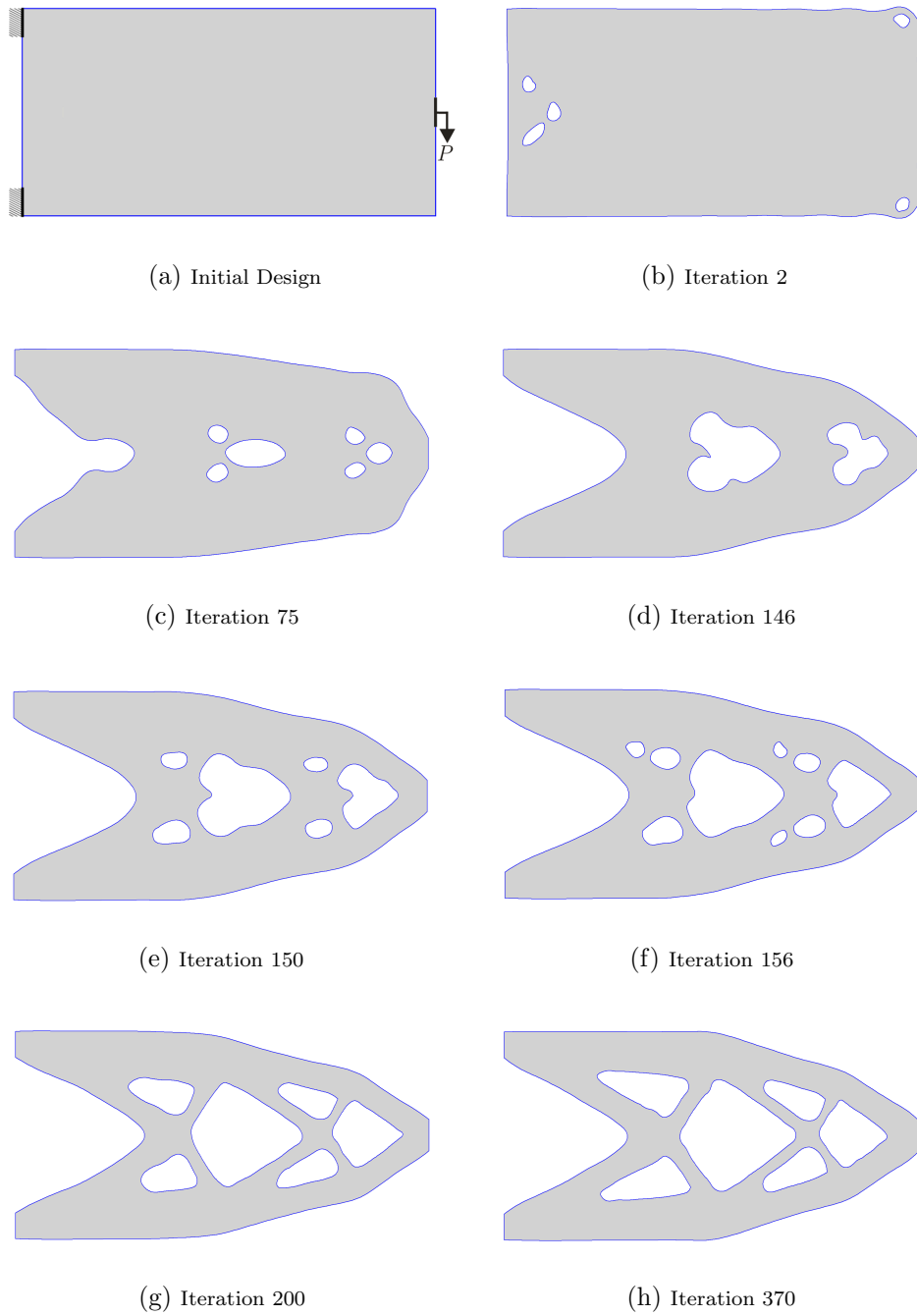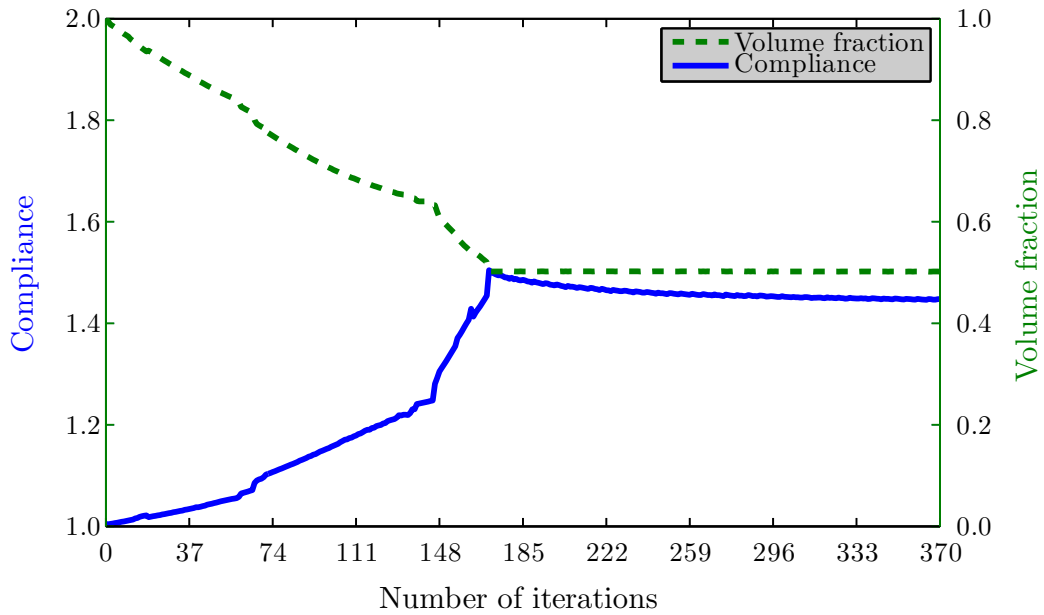(g) Iteration 46

(h) Iteration 220
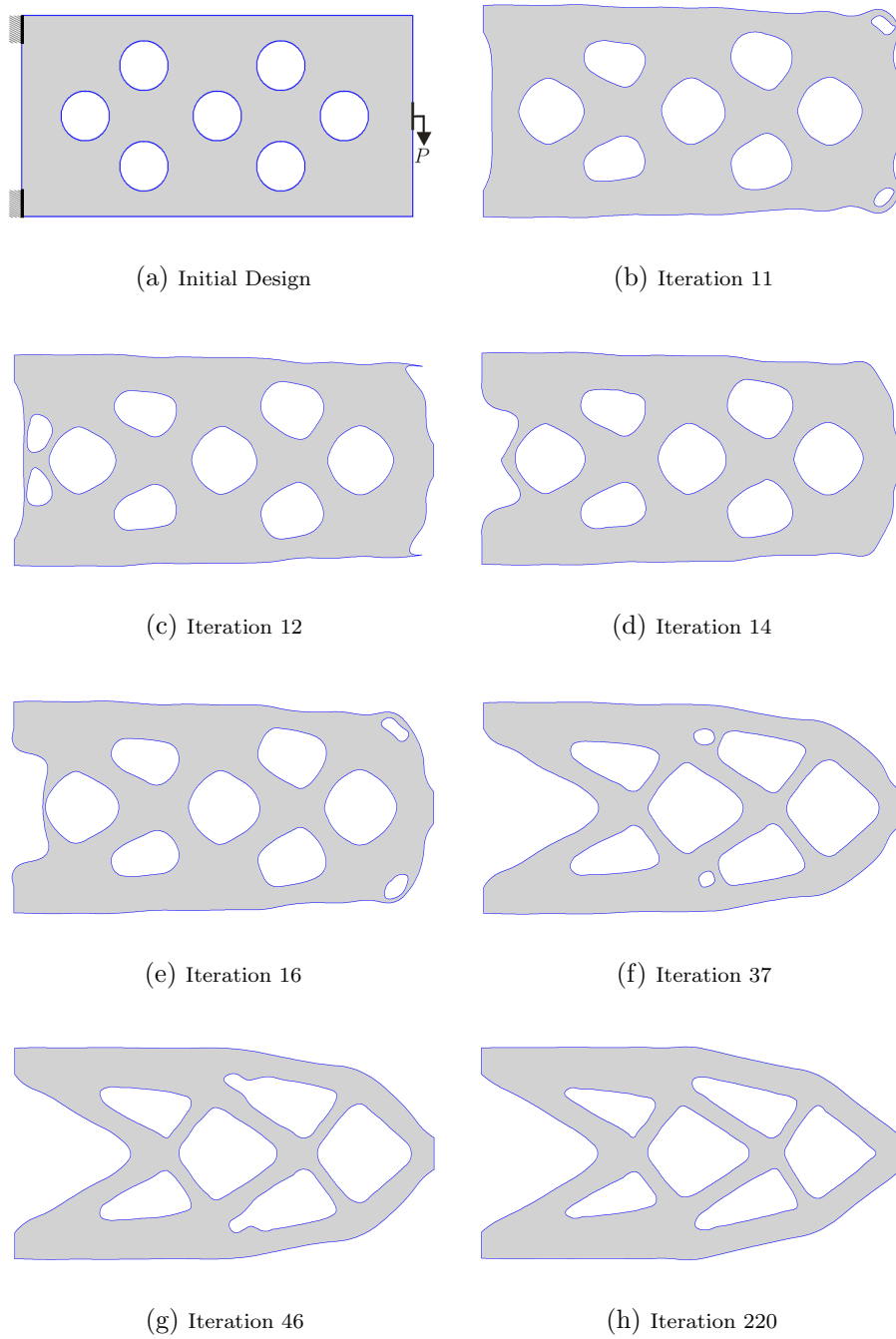
Figure 8: Evolution of structural geometry for Example-1, initial design with pre-existing holes and with hole insertion

Figure 9: Convergence of objective function and volume for Example-1, initial design with pre-existing holes and with hole insertion

cases in both shape and topology.

The evolution of objective function and volume of the structure in the final case of this example is depicted in Figure 11. Due to the absence of pre-existing holes the compliance of the initial design is lower than the initial two cases. The removal of material through hole insertion and boundary movements slowly decreases the volume and correspondingly increases the compliance of the structure. The maximum value of compliance recorded is 1.50 at iteration 170. Once the structure volume reaches the target volume the use of bisectioning algorithm effectively handles the volume constraint and the optimisation process is carried out at constant volume. This allows a slow reduction initially and stabilisation of the compliance structure afterwards. The optimisation process terminates with a final compliance of 1.44.

The three cases solved in this example are compared in Table 1. It is evident from this comparison that 370 iterations were used in the final case to reach the optimum solution, which are more than the first two cases. This difference in the total number of iterations can be related to the difference in

24

(a) Initial Design

(b) Iteration 2

(c) Iteration 75

(d) Iteration 146

(e) Iteration 150

(f) Iteration 156

(g) Iteration 200

(h) Iteration 370

Figure 10: Evolution of structural geometry for Example-1, initial design without holes and with hole insertion

25

Figure 11: Convergence of objective function and volume for Example-1, initial design without holes and with hole insertion

the structural volumes at the start of the optimisation process. The compliance and topologies of the optimal solutions are very close to each other. In general, this suggests that the proposed optimisation method is insensitive to the choice of initial guessed designs used; and does not rely on an initial guessed design with pre-existing holes as compared to the BEM and LSM based optimisation methods presented in [9, 17]. Therefore, the addition of a hole insertion mechanism is a clear advantage of this approach over the available BEM and LSM based optimisation methods.
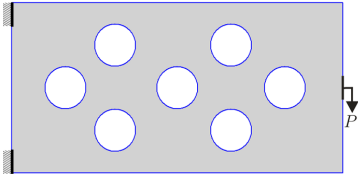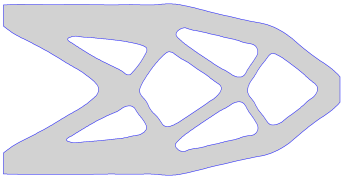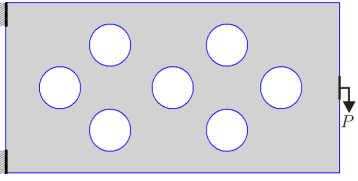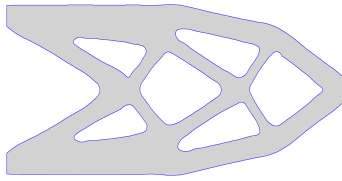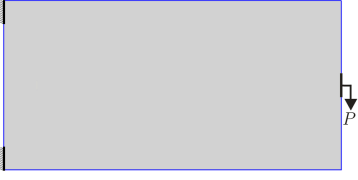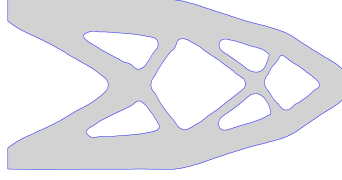
Initial Design	Final Design	N	$J(u)$	HI
		220	1.42	OFF
		220	1.43	ON
		370	1.44	ON

Table 1: Results comparison with different initial designs and hole insertion options for Example-1; N: Total number of iterations, HI: Hole insertion option (ON/OFF)

6.2. Example-2

In the second example, the minimum compliance problem is solved for a cantilever beam with an aspect ratio of 1.6:1, using initial guessed designs with and without pre-existing holes. The zero displacement boundary conditions are prescribed at the top and bottom portions of the left hand edge and the structure is loaded at the right hand side of the bottom edge as shown in Figure 12(a). The specified target volume fraction for this example is $V = 0.35V_0$. The level set design domain is discretised with 60×36 square cells.

In the first case of this example, an initial guessed design with pre-existing holes is considered for the solution of minimum compliance problem with the hole insertion option is switched OFF. As the initial volume is far away from the target volume, a fixed ℓ is used up to a pre-specified volume, i.e. $0.4V_0$. Afterwards, an exact ℓ is calculated at each optimisation step with the bisectioning algorithm. The evolution of structural geometry during the optimisation process comprised of boundary movements, hole merging with the boundary and each other, as depicted in Figure 12. The optimal design shown in Figure 12(f) is very similar to optima published in the literature, e.g. [4, 9].

Figure 13 shows convergence histories of the objective function and the volume constraint throughout the optimisation iterations. In the initial 15 iterations, the volume decreases rapidly and as a result of the material removal the objective function is raised from 0.85 to 1.04. In the following iterations, the compliance rises further to a maximum value of 1.40 at iteration 26, and then decreases steadily at constant volume. In the subsequent iterations peaks can be observed around iterations 43, 70, 230 and 310, respectively, mainly caused by a significant change of topology resulting from the elimination of one or more structural members in one iteration (related to hole merging), as can be seen from Figure 12(c-e). Afterwards, the objective function remains stable with a value of 0.96 until the end of the optimisation process.

To demonstrate the hole insertion capability and shape optimisation simultaneously, in the second case of this example, the optimisation process starts from an initial design completely filled with material, as shown in Figure 14(a). A typical value of $f_T = 1.5$ is used in this example. Nucleation of new holes can be observed in Figure 18(b), (c) and (d). The fixed and exact combination of ℓ is used during the optimisation process. The evolution of structural geometry at various stages of the optimisation process is depicted

(a) Initial Design

(b) Iteration 23

(c) Iteration 50

(d) Iteration 200
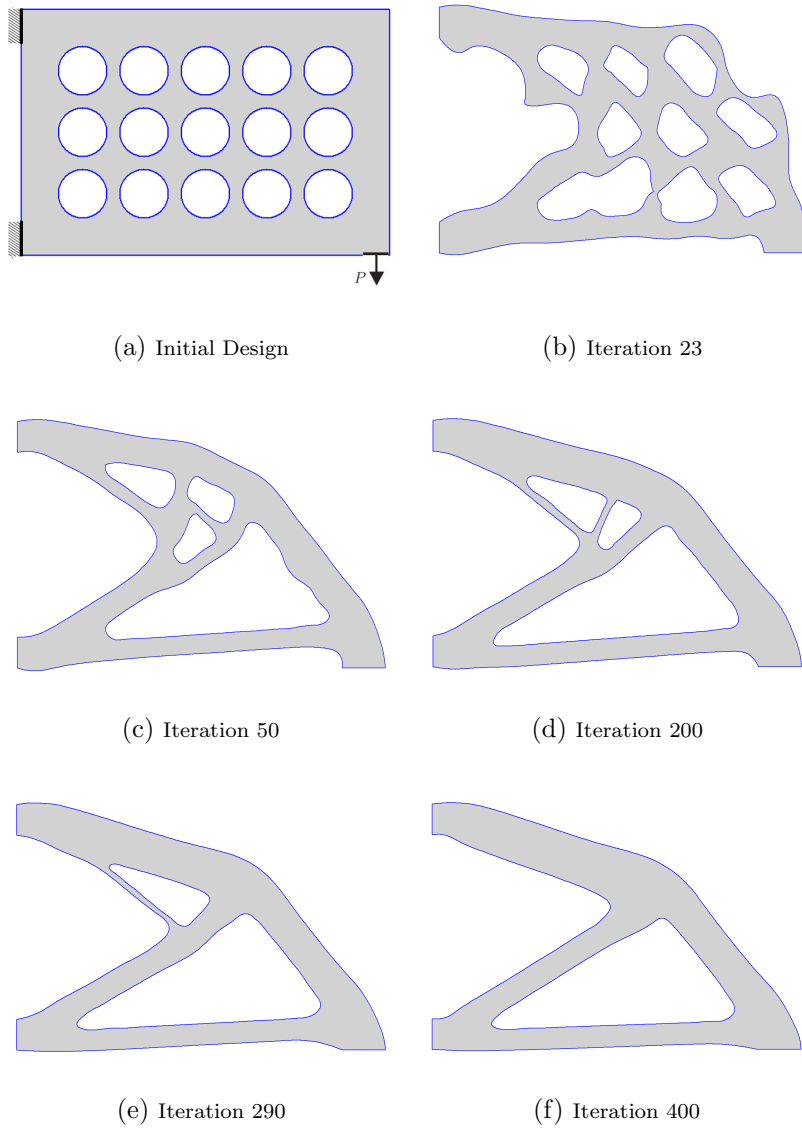
(e) Iteration 290

(f) Iteration 400

Figure 12: Evolution of structural geometry for Example-2, initial design with pre-existing holes and without hole insertion
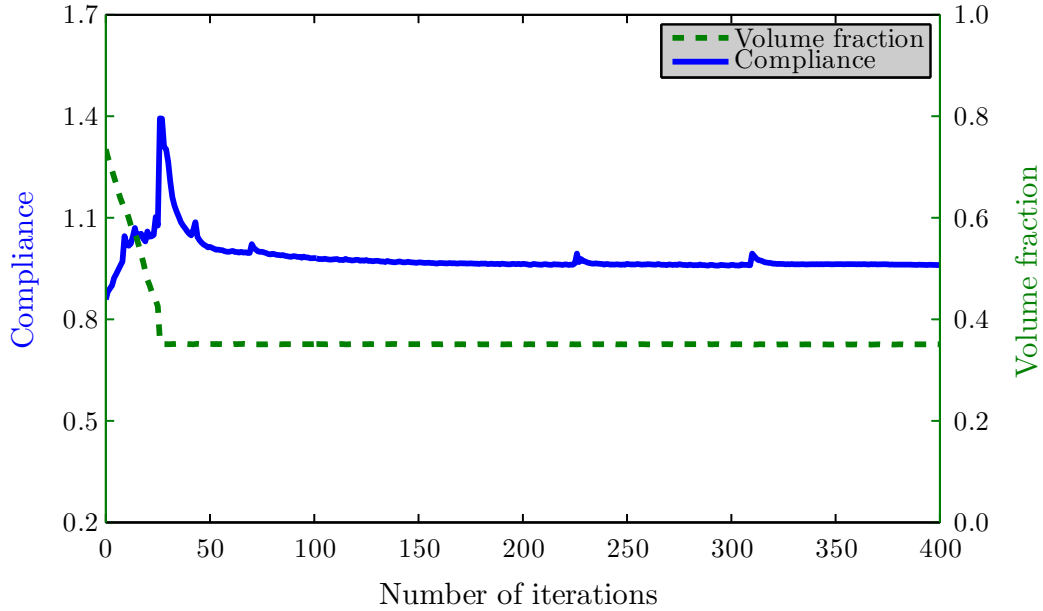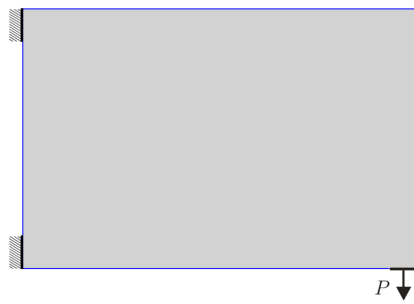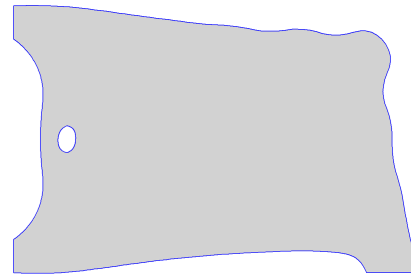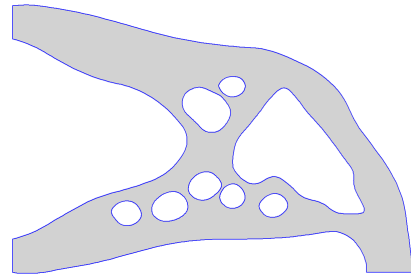
Figure 13: Convergence of objective function and volume for Example-2, initial design with pre-existing holes and without hole insertion

in Figure 14. The optimisation process comprised of hole insertion, evolution of both external and internal boundaries, and merging of holes with each other and with the boundary. Hence, both shape and topology optimisation take place simultaneously during the solution of the minimum compliance problem.

The evolution of the objective function and structural volume during the optimisation process are depicted in Figure 15. Due to a completely filled design domain, the optimisation process starts from a minimum value of the objective function, i.e. 0.45. Then it slowly increases as a result of the material removal through boundary movements and hole insertion. A high peak can be observed at iteration 103, which is mainly related to the removal of material through a slightly large hole insertion. The use of the bisectioning algorithm near the target volume fraction raises the compliance to a maximum value of 1.32 at iteration 115. Afterwards, the volume constraint is satisfied; however some peaks can be observed up to iteration 200, which are related to the removal of structural member through hole merging. Finally, the objective function is gradually reduced to 0.96 and the optimisation
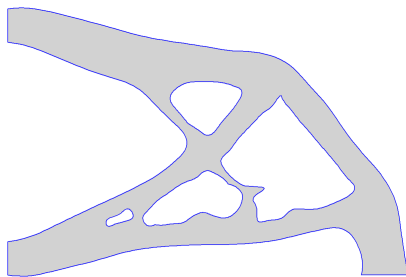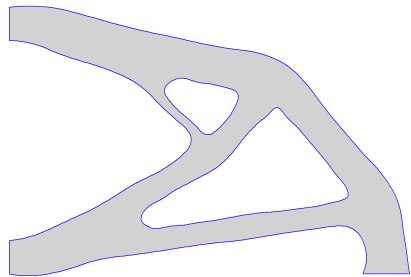
30

(a) Initial Design

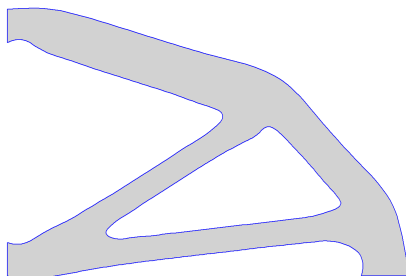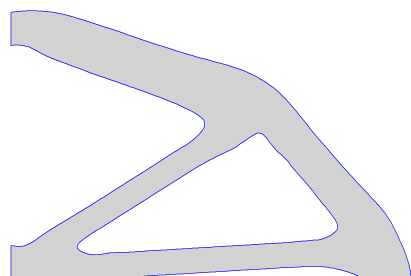(b) Iteration 40
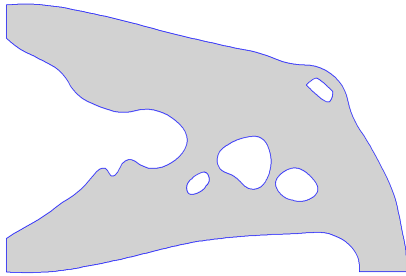
(c) Iteration 100

(d) Iteration 120

(e) Iteration 130

(f) Iteration 150

31

(g) Iteration 300

(h) Iteration 600

Figure 14: Evolution of structural geometry for Example-2, initial design without pre-existing holes and with hole insertion
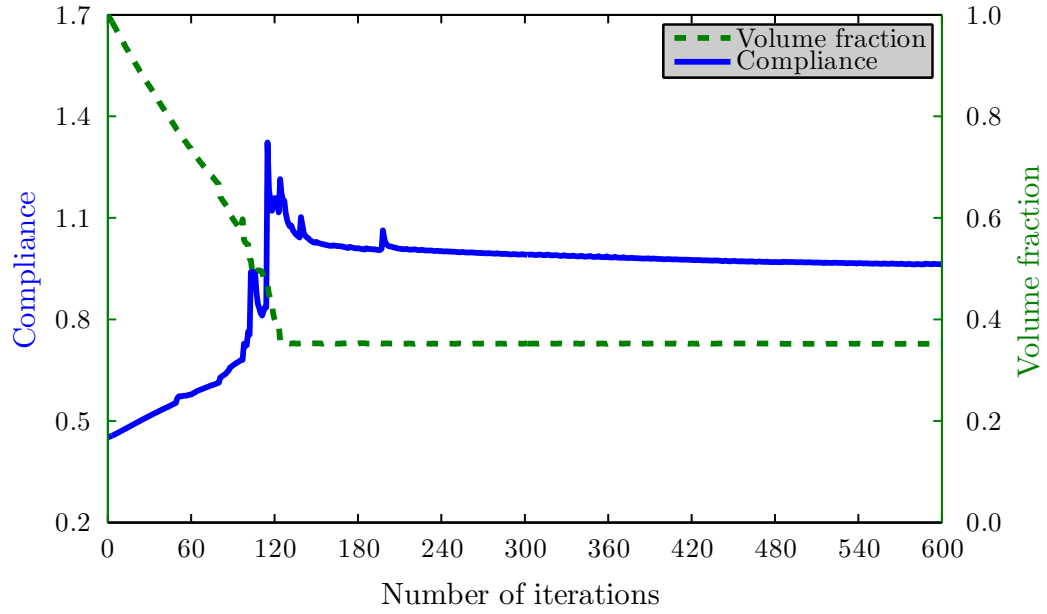
terminates at iteration 600.

Figure 15: Convergence of objective function and volume for Example-2, initial design without pre-existing holes and hole insertion

A comparison of the optimal solutions in both cases of this example is presented in Table 2. The optimal topologies and the compliances are in close agreement to each other. As observed in the previous example, the difference in the number of iterations to reach the optimal solution can also be linked to the different initial guessed designs used and their associated volumes.
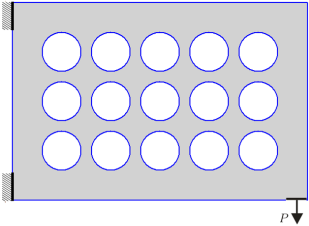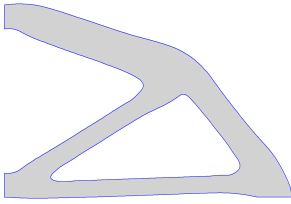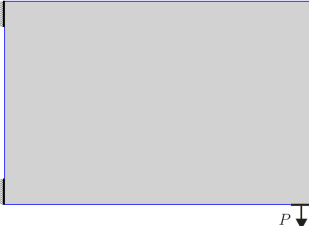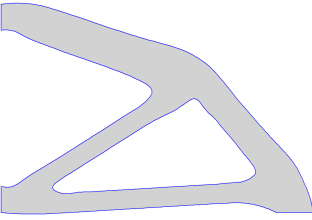
Initial Design	Final Design	N	$J(u)$	HI
		400	0.96	OFF
		600	0.96	ON

Table 2: Results comparison with different initial designs and hole insertion options for Example-2; N: Total number of iterations, HI: Hole insertion option (ON/OFF)

6.3. Example-3

The minimum compliance problem in this example is solved for a cantilever beam with an aspect ratio of 1.5:1. The specified target volume fraction for this example is $V = 0.35V_0$. The level set design domain is discretised with 60×40 square cells. Two different initial guessed designs (i.e. with and without pre-existing holes) are used for the solution of the minimum compliance problem. Further, the hole insertion option is switched OFF in the first case and switched ON in the second case, respectively.

In case 1, the optimisation process starts from an initial guess design as shown in Figure 16(a). The zero displacement boundary conditions are prescribed at the top and bottom of the left hand edge and the structure is loaded at the centre of the right hand edge. The evolution of the structural geometry at different stages of the optimisation process and the optimal design are depicted in Figure 16(b-f). It is evident from the results displayed, that some holes merge automatically with each other and with the outer boundary during the course of the optimisation process.

The convergence histories of the objective function and the structural volume are depicted in Figure 17. The initial structural volume is $V = 0.73V_0$; therefore, a fixed ℓ is used in the initial iterations and the bisectioning algorithm is then used up to the end of optimisation process. In the initial iterations a low material removal rate and slow increase in the compliance correspond to boundary perturbations only. In the subsequent iterations hole merging takes place and as a result peaks can be observed at different stages of the optimisation process. The use of the bisectioning algorithm near the target volume fraction increases the compliance to 1.33 around iteration 89. Once the volume constraint is satisfied the objective function initially decreases and then stabilises at a value of 1.29 in the subsequent iterations.

To further demonstrate the hole insertion capability of the proposed optimisation approach, the minimum compliance problem is solved with an initial design domain without any holes, as shown in Figure 18(a). The value of topological derivative used in this example is $f_T = 1.5$. Nucleation of new holes at various stages is evident from the optimisation history depicted in Figure 18.

The evolution histories of the objective function and the structural volume at each optimisation iteration are depicted in Figure 19. The optimisation process starts from a minimum value of the objective function, and then it slowly increases as a result of the boundary movements and hole insertion. The high peak at iteration 51 is related to a slightly large hole insertion; the

(a) Initial Design

(b) Iteration 10

(c) Iteration 29

(d) Iteration 75

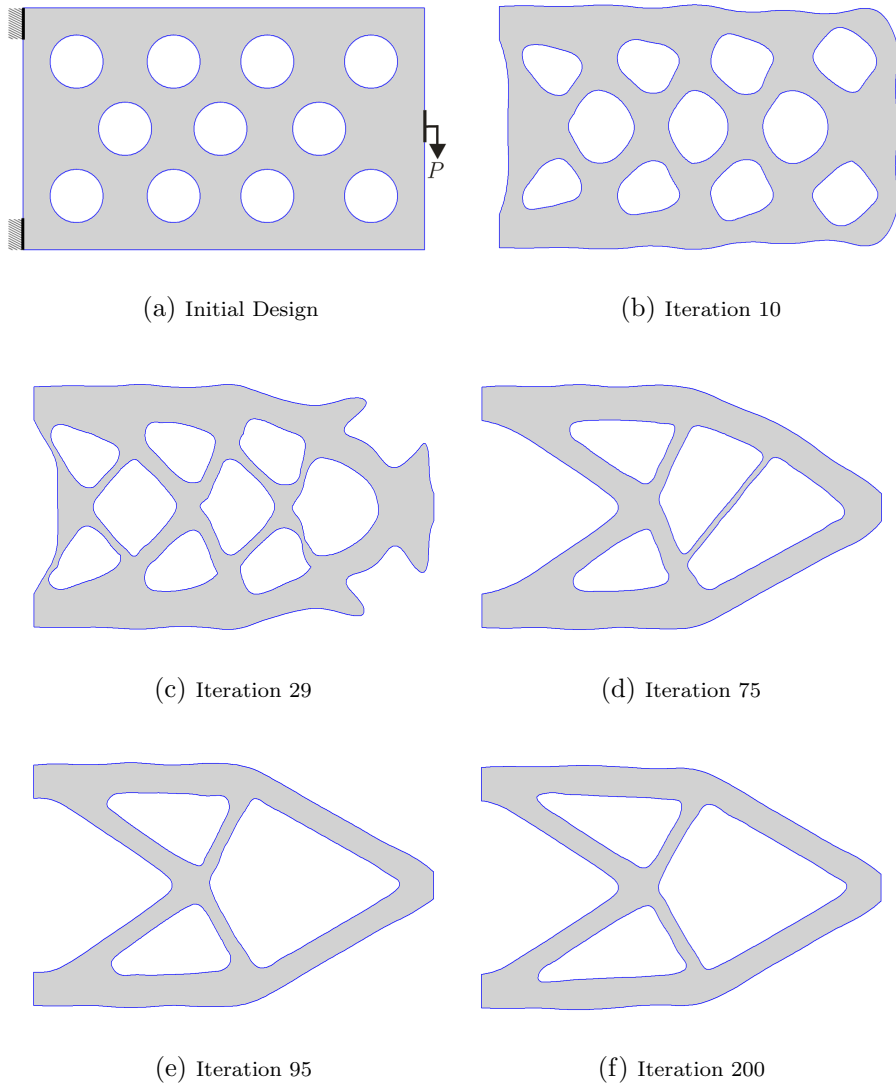(e) Iteration 95

(f) Iteration 200

Figure 16: Evolution of structural geometry for Example-3, initial design with pre-existing holes and without hole insertion
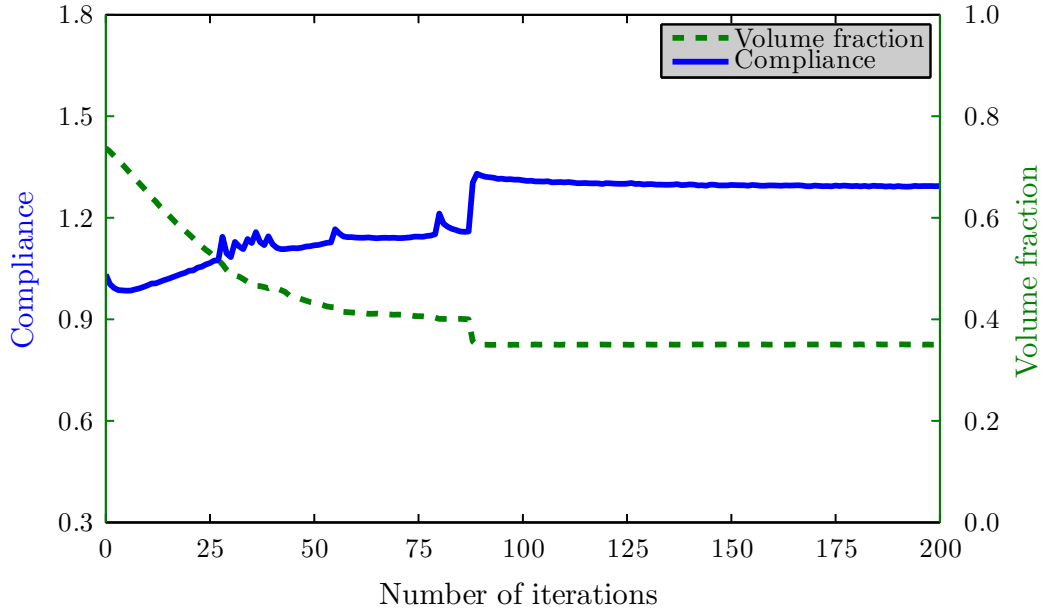
Figure 17: Convergence of objective function and volume for Example-3, initial design with pre-existing holes and without hole insertion

effect of this peak dies out in the subsequent iterations. The use of the bisectioning algorithm near the target volume fraction raises the compliance to a maximum value of 1.35 at iteration 215. Afterwards, the volume constraint is satisfied, and the objective function is reduced to 1.29 and remains stable afterwards.

In this example two different initial guessed designs are considered for the solution of the minimum compliance problem. The initial and final configurations, number of iterations, compliances and hole insertion option used in this example are compared in Table 3. It can be seen that the final optimal designs are very close to each other in both shapes, topologies and final compliances, though the initial designs are very different. In addition, the final optima are very similar to that presented in [9, 40, 41]. In addition, the proposed optimisation method provides fast convergence of the objective function and volume constraint as only 200 and 300 optimisation steps were utilised, respectively; these are less than the corresponding numbers reported in [9, 17], i.e 1500 and 2021, respectively.

36

(a) Initial Design

(b) Iteration 6

(c) Iteration 60

(d) Iteration 100
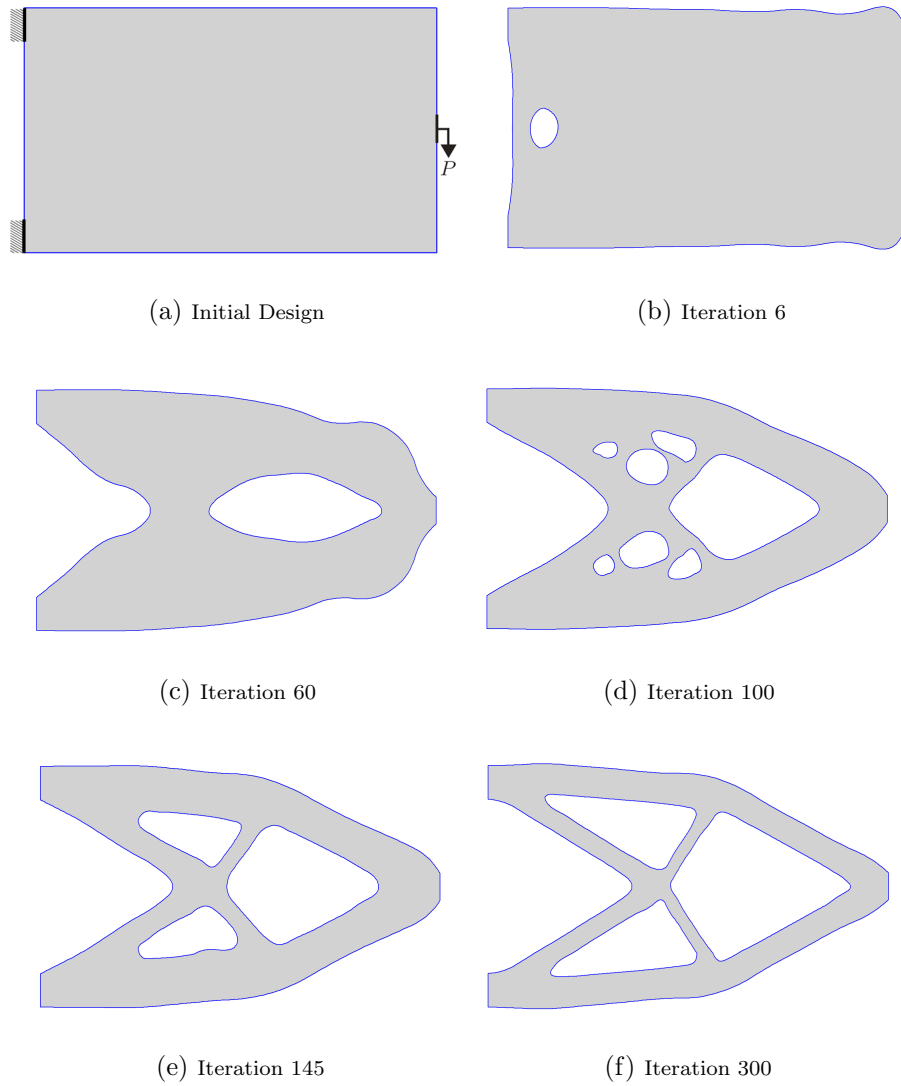
(e) Iteration 145

(f) Iteration 300

Figure 18: Evolution of structural geometry for Example-3, initial design without pre-existing holes and with hole insertion
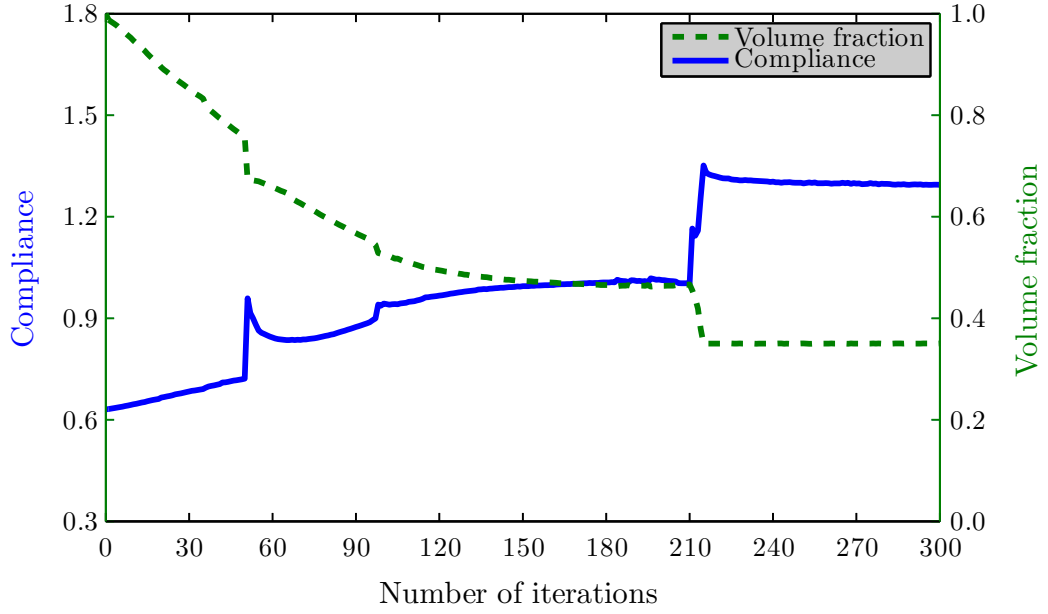
Figure 19: Convergence of objective function and volume for Example-3, initial design without pre-existing holes and with hole insertion
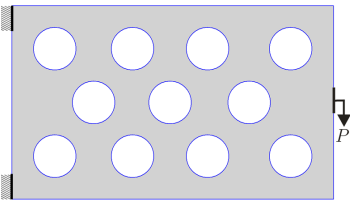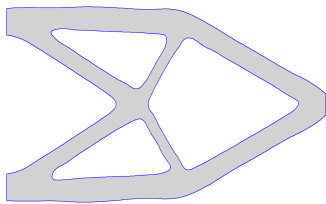
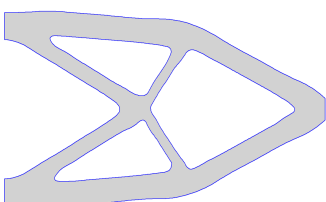| Initial Design	Final Design	N	$J(u)$	HI
		200	1.29	OFF
		300	1.29	ON

Table 3: Results comparison with different initial designs and hole insertion options for Example-3; N: Total number of iterations, HI: Hole insertion option (ON/OFF)

38

6.4. Example-4

The final example considered in this study is the Michell's type structure as shown in Figure 20(a) with an aspect ratio of 2:1. Zero displacement boundary conditions are applied in all directions at the left hand side, and the load is applied at the middle of the bottom edge. The right hand side of the bottom edge is constrained in the vertical direction and is allowed to move in the horizontal direction. The level set design domain is discretised with 80×40 square cells. The minimum compliance problem is solved for a target volume of $V = 0.35V_0$.

(a) Initial Design

(b) Iteration 20

(c) Iteration 40

(d) Iteration 69
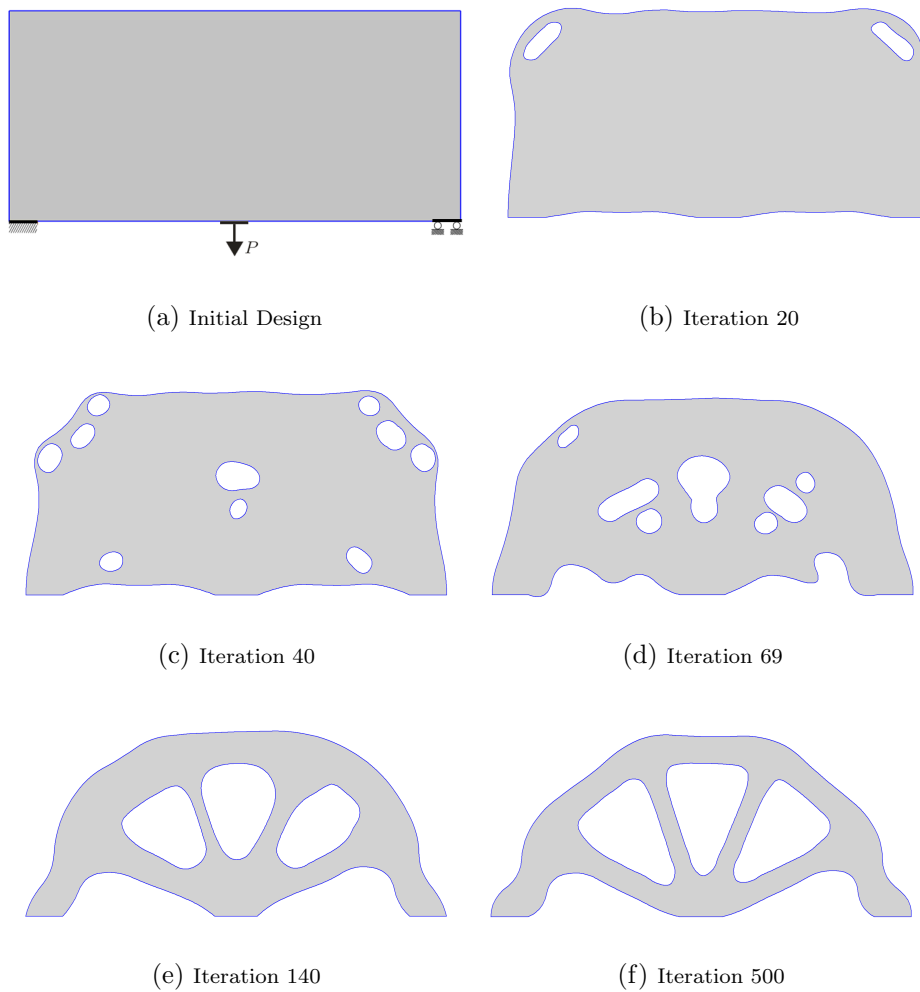
(e) Iteration 140

(f) Iteration 500

Figure 20: Evolution of structural geometry for Example-4

An initial design without pre-existing holes is considered in this example and the hole insertion option is switched ON. The optimisation problem for the minimum compliance is solved with a fixed and exact combination of ℓ. Nucleation of holes can be observed throughout the optimisation process. The evolution of the structural geometry at different stages of the optimisation process and the final optimal design is depicted in Figures 20(b)-(e). The final optimum as shown in Figure 20(f) is very similar to that presented in [9].

The evolution of the objective function and structural volume are depicted in Figure 21. The use of a fixed ℓ and nucleation of holes provides a smooth progression of the objective function and volume constraint. Once the volume constraint converges around iteration 150, the subsequent iterations, relatively large in number, are used to carry out shape optimisation only and this results in material re-distribution within the design domain. It can be seen that once the volume constraint is satisfied the objective function initially decreases and then stabilises at a value of 0.24 in the following iterations. The proposed optimisation method provides fast convergence of the objective function and volume constraint as only 500 optimisation steps are used in this example, which are less than the 2023 iterations utilised in [9] for a similar problem.
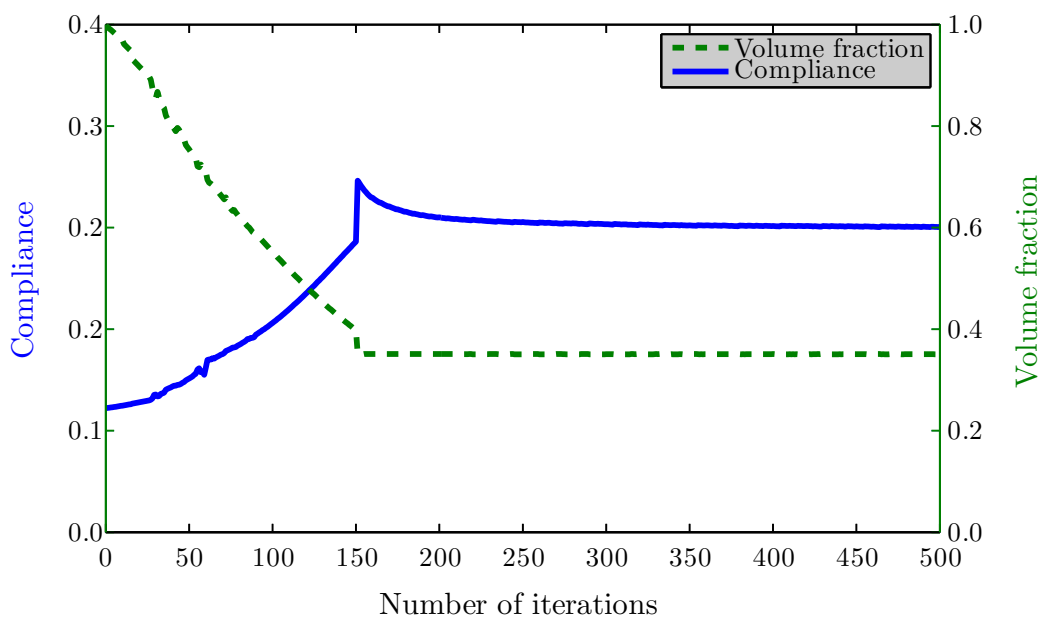
Figure 21: Convergence of objective function and volume for Example-4

7. Conclusions

A sensitivity analysis, BEM, LSM and NURBS based topology optimisation method is proposed in this paper. The proposed optimisation method is further equipped with a topological derivative based hole insertion mechanism, which allows nucleation of new holes inside the design domain, and substantially overcomes the deficiency of a hole insertion mechanism in the previously presented BEM and LSM based optimisation methods, i.e. [9, 17]. The integration of topological and shape sensitivity derivatives provides an optimisation technique using which both shape and topology optimisation can be performed at the same time efficiently and robustly. During the numerical implementation, it has been observed that for a given problem the proposed optimisation method provides very similar optimal solutions with different initial designs.In the current implementation, the use of a bisectioning algorithm allows accurate calculations of the Lagrange multiplier, which exactly satisfies the volume constraint, and thus provides smooth convergence of the objective function.

Numerical examples of four different types of two-dimensional structures are chosen to show the success, computational efficiency (gained through boundary discretisation), convergence speed and insensitivity to initial designs. Compared with the available BEM and LSM based optimisation methods, the present method generates similar optimal designs rapidly and largely eliminates the dependency on initial guessed designs with pre-existing holes. In addition, the use of NURBS provides optimal designs in a standard CAD format without any intermediate material densities along the structural boundary. Therefore, from an engineering point of view the optimal design can be easily interpreted and be directly used in other design processes.

Acknowledgements

References

[1] S. Osher, J. A. Sethian, Front propagating with curvature-dependent speed: algorithms based on Hamilton-Jacobi formulations, Journal of Computational Physics 79 (1) (1988) 12–49.

[2] J. A. Sethian, A. Wiegmann, Structural boundary design via level set and immersed interface methods, Journal of Computational Physics 163 (2) (2000) 489–528.

[3] S. J. Osher, F. Santosa, Level set methods for optimization problems involving geometry and constraints: I. frequencies of a two-density in-homogeneous drum, Journal of Computational Physics 171 (1) (2001) 272 – 288.

[4] M. Y. Wang, X. Wang, D. Guo, A level set method for structural topology optimization, Computer Methods in Applied Mechanics and Engineering 192 (1-2) (2003) 227–246.

[5] G. Allaire, F. Jouve, A. M. Toader, Structural optimization using sensitivity analysis and a level-set method, Journal of Computational Physics 194 (1) (2004) 363–393.

[6] N. P. Dijk, K. Maute, M. Langelaar, F. Keulen, Level-set methods for structural topology optimization: a review, Structural and Multidisciplinary Optimization 48 (3) (2013) 437–472.

[7] O. Sigmund, J. Petersson, Numerical instabilities in topology optimization: A survey on procedures dealing with checkerboards, mesh-dependencies and local minima, Structural optimization 16 (1) (1998) 68–75.

[8] G. W. Jang, Y. Y. Kim, Sensitivity analysis for fixed-grid shape optimization by using oblique boundary curve approximation, International Journal of Solids and Structures 42 (11–12) (2005) 3591–3609.

[9] S. Yamasaki, T. Yamada, T. Matsumoto, An immersed boundary element method for level-set based topology optimization, International Journal for Numerical Methods in Engineering 93 (9) (2013) 960–988.

[10] S. Y. Wang, K. M. Lim, B. C. Khoo, M. Y. Wang, An extended level set method for shape and topology optimization, Journal of Computational Physics 221 (1) (2007) 395–421.

[11] J. Luo, Z. Luo, L. Chen, L. Tong, M. Y. Wang, A semi-implicit level set method for structural shape and topology optimization, Journal of Computational Physics 227 (11) (2008) 5561–5581.

[12] S. Wang, M. Y. Wang, A moving superimposed finite element method for structural topology optimization, International Journal for Numerical Methods in Engineering 65 (11) (2006) 1892–1922.

[13] T. Fries, T. Belytschko, The extended/generalized finite element method: An overview of the method and its applications, International Journal for Numerical Methods in Engineering 84 (3) (2010) 253–304.

[14] T. Belytschko, S. P. Xiao, C. Parimi, Topology optimization with implicit functions and regularization, International Journal for Numerical Methods in Engineering 57 (8) (2003) 1177–1196.

[15] L. Van Miegroet, P. Duysinx, Stress concentration minimization of 2D filets using X-FEM and level set description, Structural and Multidisciplinary Optimization 33 (4-5) (2007) 425–438.

[16] P. Wei, M. Y. Wang, X. Xing, A study on X-FEM in continuum structural optimization using a level set model, Comput-Aided Design 42 (8) (2010) 708–719.

[17] K. Abe, S. Kazama, K. Koro, A boundary element approach for topology optimization problem using the level set method, Communications in Numerical Methods in Engineering 23 (5) (2007) 405 – 416.

[18] K. Abe, T. Fujiu, K. Koro, A be-based shape optimization method enhanced by topological derivative for sound scattering problems, Engineering Analysis with Boundary Elements 34 (12) (2010) 1082 – 1091.

[19] S. Ha, S. Cho, Level set based topological shape optimization of geometrically nonlinear structures using unstructured mesh, Computers and Structures 86 (13–14) (2008) 1447–1455.

[20] S. Yamasaki, T. Nomura, A. Kawamoto, K. Sato, S. Nishiwaki, A level set-based topology optimization method targeting metallic waveguide design problems, International Journal for Numerical Methods in Engineering 87 (9) (2011) 844–868.

[21] S. Yamasaki, S. Nishiwaki, T. Yamada, K. Izui, M. Yoshimura, A structural optimization method based on the level set method using a new geometry-based re-initialization scheme, International Journal for Numerical Methods in Engineering 83 (12) (2010) 1580–1624.

[22] B. Ullah, J. Trevelyan, P. Matthews, Structural optimisation based on the boundary element and level set methods, Computers & Structures 137 (2014) 14–30.

[23] B. Ullah, J. Trevelyan, Correlation between hole insertion criteria in a boundary element and level set based topology optimisation method, Engineering Analysis with Boundary Elements 37 (11) (2013) 1457 – 1470.

[24] B. Ullah, J. Trevelyan, I. Ivrissimtzis, A three-dimensional implementation of the boundary element and level set based structural optimisation, Engineering Analysis with Boundary Elements 58 (2015) 176–194.

[25] A. A. Novotny, R. A. Feijóo, E. Taroco, C. Padra, Topological sensitivity analysis for three-dimensional linear elasticity problem, Computer Methods in Applied Mechanics and Engineering 196 (41) (2007) 4354–4364.

[26] L. Carretero Neches, A. P. Cisilino, Topology optimization of 2D elastic structures using boundary elements, Engineering Analysis with Boundary Elements 32 (7) (2008) 533–544.

[27] D. F. Rogers, An Introduction to NURBS: With Historical Perspective, Morgan Kaufmann, 2001.

[28] J. Trevelyan, "Concept Analyst Ltd". [Online] .www.conceptanalyst.com (2006). [link].
URL www.conceptanalyst.com

[29] C. A. M. Soares, K. K. Choi, Boundary elements in shape optimal design of structures, in: The Optimum Shape, General Motors Research Laboratories Symposia Series, Springer US, 1986, pp. 199–231.

[30] B. N. Pshenichny, J. M. Danilin, Numerical Methods in External Problems, Moscow: MIR Publishers, 1978.

[31] P. D. Dunning, H. A. Kim, A new hole insertion method for level set based structural topology optimization, International Journal for Numerical Methods in Engineering 93 (1) (2013) 118–134.

[32] A. A. Becker, The Boundary Element Methods in Engineering: A complete course, McGRAW - HILL BOOK COMPANY, 1992.

[33] A. A. Novotny, R. A. Feijóo, E. Taroco, C. Padra, Topological sensitivity analysis, Computer Methods in Applied Mechanics and Engineering 192 (7) (2003) 803–829.

[34] R. J. Marczak, Optimization of elastic structures using boundary elements and a topological-shape sensivity formulation, Latin American Journal of Solids and Structures 5 (2008) 99–117.

[35] S. Wang, M. Y. Wang, Radial basis functions and level set method for structural topology optimization, International Journal for Numerical Methods in Engineering 65 (12) (2006) 2060–2090.

[36] O. Sigmund, A 99 line topology optimization code written in Matlab, Structural and Multidisciplinary Optimization 21 (2) (2001) 120–127.

[37] D. Adalsteinsson, J. A. Sethian, The fast construction of extension velocities in level set methods, Journal of Computational Physics 148 (1) (1999) 2–22.

[38] J. A. Sethian, Level Set Methods and Fast Marching Methods: Evolving Interfaces in Computational Geometry, Fluid Mechanics, Computer Vision, and Materials Science, 2nd Edition, Cambridge University Press, 1999.

[39] D. Adalsteinsson, J. A. Sethian, A fast level set method for propagating interfaces, Journal of Computational Physics 118 (2) (1995) 269–277.

[40] T. Yamada, K. Izui, S. Nishiwaki, A. Takezawa, A topology optimization method based on the level set method incorporating a fictitious interface energy, Computer Methods in Applied Mechanics and Engineering 199 (45-48) (2010) 2876–2891.

[41] E. Cervera, J. Trevelyan, Evolutionary structural optimisation based on boundary representation of NURBS. Part I: 2D algorithms, Computers and Structures 83 (2005) 1902–1916.

[42] Marc Bonnet, B. Guzina, Sounding of finite solid bodies by way of topological derivative, International Journal for Numerical Methods in Engineering 61 (2004) 2344–2373.

[43] Marc Bonnet, N. Nemitz, FM-BEM and topological derivative applied to inverse acoustic scattering. M. Schanz, O. Steinbach. Boundary element analysis: mathematical aspects and applications (2007) 87–212.

[44] N. Nemitz, Marc Bonnet, Topological sensitivity and FMM-accelerated BEM applied to 3D acoustic inverse scattering, Engineering Analysis with Boundary Elements 32 (2008) 957–970.

[45] H. Isakari, K. Kuriyama, S. Harada, T. Yamada, T. Takahashi, T. Matsumoto, A topology optimisation for three-dimensional acoustics with the level set method and the fast multipole boundary element method, Mechanical Engineering Journal 1 (4) (2014) 1–13.

[46] S. Garreau, P. Guillaume, M. Masmoudi, The topological asymptotic for PDE systems: The elasticity case, SIAM Journal on Control and Optimization 39 (6) (2001) 1756–1778.